Characterizing the Fatigue Damage in Non-Traditional Laminates of Carbon Fiber Composites Using Radiography

A Thesis
Presented to
The Academic Faculty

by

Joshua Rast

In Partial Fulfillment
of the Requirements for the Degree
of Masters in Mechanical Engineering in the
George W. Woodruff School of Mechanical Engineering

Georgia Institute of Technology
May 2009

Characterizing the Fatigue Damage in Non-Traditional Laminates of Carbon Fiber Composites Using Radiography

Approved by:

Dr. W. Steven Johnson, Advisor
Schools of Mechanical Engineering/Materials Science
Georgia Institute of Technology

Dr. Erian Armanios
School of Aerospace Engineering
Georgia Institute of Technology

Dr. Rick Neu
School of Mechanical Engineering
Georgia Institute of Technology

Date Approved:

ACKNOWLEDGEMENTS

I would like to thank my advisor, Dr. Steve Johnson, for his invaluable guidance throughout the course of this project. I would like to thank Rick Brown for his help in setting up and maintaining the test frames.

TABLE OF CONTENTS

LIST OF TABLES

Page

LIST OF FIGURES

Page

NOMENCLATURE

a	Crack/Notch half length
ASTM	American Society for Testing and Materials International
C	Compliance
E	Modulus of Elasticity, Stiffness
E_s	Static Stiffness
E_{xy}	In-plane Residual Fatigue Shear Stiffness
E_{xz}	Out-of-plane Shear Stiffness
FH	Filled Hole
FH-HC	Filled Hole Testing with Half Clamped fasteners
FHC	Filled Hole Compression (R=-10)
FHT	Filled Hole Tension (R=-0.1)
Fully Reversed	R=-1
G	Strain Energy Release Rate
G_C	Fracture Energy
G_I	Mode I energy release rate
G_s	Energy Absorbed per Unit Split
G_d	Energy Absorbed per Unit Delamination
k	Interlaminar Shear Strength
K	Stress Ratio

K_I	Mode I stress intensity factor
K_{IC}	Mode I critical stress intensity factor
ΔK	Stress Intensity Factor
L	Length
LEFM	Linear Elastic Fracture Mechanics
LSS	Laminate Stacking Sequence
Mostly Tension	R=-0.35
Mostly Compression	R=-3
N, n	Number of Cycles
N_f	Fatigue Life in Cycles
OH	Open Hole
OHC	Open Hole Compression (R=-10)
OHT	Open Hole Tension (R=-0.1)
P	Load
R ratio, R	Minimum Stress divided by Maximum Stress
R	Residual Strength
R_s	Static Strength
R, r	Notch/crack radius
Sxy	In-plane Residual Shear Fatigue Strength
Sxz	Out-of-plane Shear Strength
Syz	Out-of-plane Shear Residual Strength
Vf	Fiber Volume Fraction
W	Width

x	Coordinate measured from center of notch perpendicular to direction of applied load
X_c	Longitudinal Compressive Residual Fatigue Strength
X_t	Longitudinal Tensile Residual Fatigue Strength
Y_c	Transverse Compressive Residual Fatigue Strength
Y_t	Transverse Tensile Residual Fatigue Strength
δ	Material Non-Linearity Parameter
ε	Strain
ε_f	Average Strain to Failure
ϕ	Initial fiber misalignment angle
ν	Poisson's ratio
σ	Applied Axial Stress
σ_a	Alternating Stress
σ_c	Compressive Strength
σ_m	Mean Stress
σ_{max}	Maximum Stress
σ_{min}	Minimum Stress
σ_t	Tensile Strength
σ_y	Local stress component in the y-direction
σ_0	Unnotched tensile strength

General Subscripts:

m	Matrix

f	Fiber
c	Composite
x	X-Direction
y	Y-Direction
z	Z-Direction
1, 2, 3…	1-Direction, 2-Direction, 3 Direction, etc.

Laminate Notation and Abbreviation:

Numbers Denote Fiber Angle Relative to the Longitudinal Axis

Subscript Numbers Denote Multiple Layers

Subscript s Denotes a Symmetric Laminate

80/10/10	$[0_4/45/0_3/90/0]_s$	As: (% of 0)/(% of 45)/(% of 90)
50/40/10	$[45/90/-45/0_2/45/0_2/-45/0]_s$	As: (% of 0)/(% of 45)/(% of 90)
80/20	$[\pm5/65/(\pm5)_2/-65/\pm5]_s$	As: (% of ±5)/(% of ±65)
70/30	$[\pm5/65/(\pm5)_2/-65/5/65]_s$	As: (% of ±5)/(% of ±65)

Chapter 1 : INTRODUCTION

1.1 Abstract

The goal of this academic project was to study the effects of different variables on the damage progression around a central hole in carbon fiber composite coupon specimens. The tracked variables included the type of layup, stress ratio, stress levels, and damage mechanisms observed in each specimen. In-situ x-ray of the individual laminates recorded the extent of damage, mostly longitudinal splitting, as a function of the cycle count. The following lay-ups were included in the experiment: $[45/90/-45/0_2/45/0_2/-45/0]_s$, $[\pm5/65/(\pm5)_2/-65/\pm5]_s$, and $[\pm5/65/(\pm5)_2/-65/5/65]_s$.

More specifically, the objective of this study was to determine the stress levels at which detectable damage started to develop. The researchers chose to apply 50,000 cycles at each stress level and once damage was detected, the stress level was typically raised by 34.5 MPa (5 KSI), and then cycled another 50,000 cycles until damage exceeding 1.27 cm (0.50”) in length was observed. Once the damage exceeded 1.27 cm (0.50”), cycling was continued to 1,000,000 cycles. Upon completion of the fatigue cycling, each specimen’s residual strength was determined. The damage length versus stress level was plotted as a way to compare damage onset stresses and growth as a function of lay-up and stress ratio.

Key Words: non-traditional lay-ups, damage, notched composites, off-axis plies

1.2 Introduction

This research focused on the fatigue of non-traditional laminates, in which off-axis plies replaced the longitudinal 0° plies of traditional laminates. In all cases, these off-axis plies can lead to entirely new laminates without any 0°, 45°, or 90° plies in them as shown by P.J. Treasurer at the Georgia Institute of Technology in 2006 [1]. In 1999, P. Berbinau thought a minimal reduction in strength would hopefully be offset by a marked increase in the structure's resistance to crack propagation, which is its damage resistance [2]. This is of interest for many reasons including the extensive use of composites as structural components in aircraft, with multiple holes used for joints and other connections. During the testing phase, each specimen was monitored for several modes of damage – specifically longitudinal splitting, matrix cracking, and delamination both at the surface (fiber pulloff from off-axis plies) and traditional delamination found near the middle of the stacking sequence. However, the primary damage found during the testing was longitudinal splitting. Damage was measured through the use of in-situ x-ray with a penetrating dye, and recorded as the greatest longitudinal distance between the furthermost crack tips.

Chapter 2 : BACKGROUND

Information concerning fatigue of composites can be separated into useful knowledge about the experimental approach or information about modeling fatigue damage. This following section will discuss the experimental approach and characterization of fatigue mechanisms and variables, and that will be followed by examples of modeling approaches.

2.1 Experimental Approach

Due to their complex geometry and the behavior of their constituents, composites require extensive testing to guarantee a successful design of a component or structure. This testing is embedded into the entire design phase and spans from the creation of the constituents and resulting lamina, all the way to the desired structural level. In order to ensure the data obtained is useful for comparison, and provides repeatable and reliable results, rigorous standards outline the testing procedures. In the realm of fatigue testing, the goal is to acquire meaningful data without unnecessarily wasting time or samples.

The behavior of composite laminates in various ratios of tension fatigue and compression fatigue (for both filled hole and open hole specimens), will highlight potential benefits of non-traditional lay-ups through relatively simple and easy to implement tests.

2.1.1 Tension Fatigue

Tension fatigue of composites plays a significant role in characterizing the mechanical properties of a composite laminate. With a straightforward setup, tension

fatigue, as opposed to compression, torsional or biaxial fatigue, provides insightful data into the performance of a material under conditions that begin to approach the fidelity of real-world applications. While a material's fatigue behavior can not be completely defined by this one test (or a test matrix consisting of primarily tension fatigue), it is a step up from static tests. In industry, characterizing composites is a building block procedure. Static tests provide a baseline for ideal stiffness and strength of a composite. Tension fatigue follows, with compression fatigue being the next logical step. Eventually, full-scale structures are tested and fatigue loaded using the exact geometry as designed. Damage mechanisms are recorded and compared between the tests to aid in deciding the location and orientation of a composite laminate within a final product.

2.1.1.1 Damage Mechanisms

The complexity of designing with composites is largely due to the number of damage mechanisms that influence the properties of the material when it undergoes tensile loading. Y. Yan showed in 1999 that these often include cracks forming in the matrix, splitting occurring between the fiber and matrix, delamination between plies, and eventual breakage of the fibers [3]. Certain damages are more catastrophic than others. Matrix cracking occurs often, due to a lower strength than the fibers. Since they contribute little overall strength or stiffness to the structure, primarily preventing buckling of the fibers as well as protecting them from the environment, these cracks can extend significantly before any noticeable change in compliance or failure of the specimen is noticed. S.M. Spearing found in 1984 that splitting between the fiber and

matrix also routinely occurs at higher loads due to shear between the fiber and matrix, or delamination between different plies in the laminate [4].

2.1.1.2 Delamination and "Fiber Pull-off"

Delamination plays a large role in the fatigue performance of a composite laminate. Generally, delamination occurs in the middle plies of a laminate; however, for certain layups with off-axis plies on the outside, the fibers in those plies may "pull off" from the edges. Extensive research, by R. Talreja in 1999 and S. Kellas in 1986 and R. Barboni in 1999 [5, 6, 7], into this area has yielded two approaches to predicting this phenomenon. The first method uses a mechanics of materials basis. It determines the stress state in the composite and compares it to a failure criterion. This criterion requires only interlaminar stresses to determine the possibility for delamination. The second method applies a fracture mechanics principle - namely the strain energy release rate G. This can be found from a stress potential technique or a finite element analysis approach with virtual crack extension or modified crack closure [7].

Delamination is never the first type of damage observed in the specimen. Before the required interlaminar stresses can be reached, the matrix must first reach the characteristic damage state, which is a saturation state for intralaminar cracking. Compared to static testing, delamination occurs at lower stress levels than those required for static failure. The matrix cracking weakens the composite and changes the boundary conditions at the laminate edge [7].

2.1.1.3 Stress Ratio

The R ratio, defined as the minimum stress over the maximum stress, significantly affects the performance of the composite in fatigue [4]. A couple examples of "R" ratios, also called stress ratios, are -0.1, -10, -1, -0.35, and -3. Stress ratio -0.1 is almost all tension, with on 10% of the load reversed into compression. -10 is the opposite, almost all compression with only 10% of the maximum compression reversing into tension. -1 has equal loads in both the tensile and compressive direction. -0.35 and -3 represent tests with approximately one-third of the loading reversing in the other direction.

2.1.2 Compression Fatigue

As opposed to metals, composites are more prone to failure in compression fatigue than in tension fatigue, as shown by A. Razvan and K. Reifsnider in 1975 [8]. This is due to an additional set of damage mechanisms present in compression which are not seen in tension. Another issue with compression fatigue is the effect of the test fixture used to combat overall buckling of the specimen.

2.1.2.1 Damage Mechanisms

The two additional damage mechanisms affecting compressive fatigue performance are microbuckling and kink banding.

Microbuckling

Microbuckling occurs when the fibers themselves begin buckling within the matrix. Two types of microbuckling exist: an extensional mode, and a shear mode. In 2000, K. Niu found that for fiber volume fractions greater than 0.3, the shear mode is the

dominant mode that determines the compressive strength of the composite [9]. Both modes are shown in Figure 2.1.

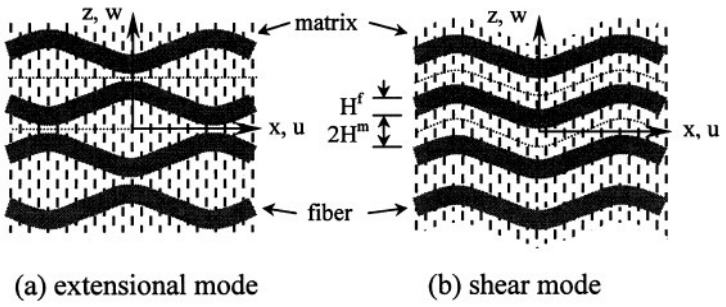

Figure 2.1 Pictorial representation of two modes of microbuckling

For composites with stiff fibers, the lamina compressive strength is given by $\sigma_1^c = \frac{G^m}{1 - v^f}$. Where the superscript "m" refers to the matrix; "f" refers to the fiber, and "c" is for the composite. Assuming an infinite fiber shear modulus, this reduces to $\sigma_1^c = G_{13}^c$. This highly overestimates the ability of the material; possible reasons are neglecting effects from nonlinear shear stiffness, initial fiber misalignment in manufacturing, or partial slipping between interfaces [9].

Kink Banding

Kink banding is another phenomenon that could occur in a composite, and it happens on a larger scale than microbuckling. Under enough compressive stress, the fibers may macroscopically kink or buckle and act as elastoplastic hinges over which the fibers crumple and break [9]. For fibers that are not properly aligned, the compressive stress of the composite is $\sigma_1^c = \frac{k}{\phi_0}$. Where "k" is the interlaminar shear strength, and ϕ_0 is the misalignment angle. For a general fiber volume fraction,

$\sigma_1^c = \frac{k^c}{\gamma_y^c + \phi_0} = \frac{G_{13}^c}{1 + \phi_0/\gamma_y^c}$ where $\gamma_y^c = k^c / G_{13}^c$. For composites with low fiber volume fractions (less than 0.3), the kink band angle approaches 45°. At more realistic ratios for carbon fiber epoxies, the angle is 20-30° [9]. This is shown in Figure 2.2.

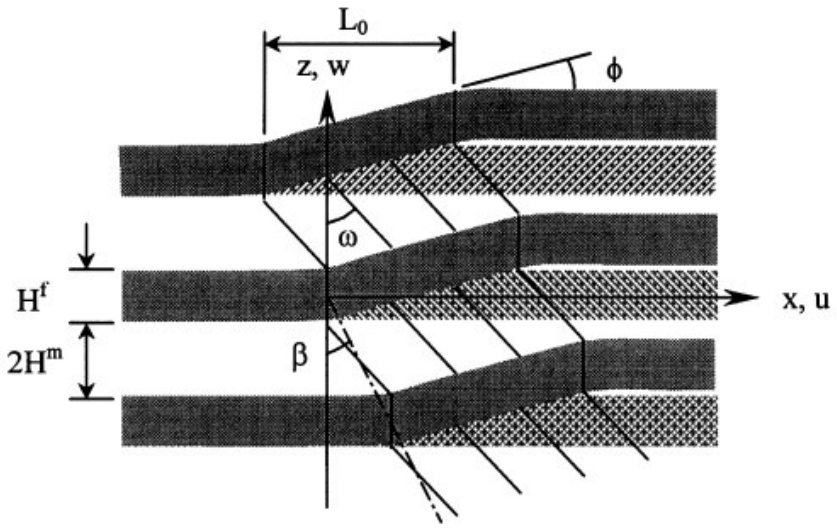

Figure 2.2 Kink-Banding in a typical composite

2.1.2.2 Test Fixtures

Due to global buckling problems when testing specimens in compression, compression test fixtures must be utilized for both compression fatigue and for determining residual compression strength. Ideally, the fatigue test fixture would not carry any of the load by clamping the specimen and allowing the load to be partially carried by the fixture.

For 30.48 x 3.81 cm (12” x 1.5”) coupon specimens, the residual strength test fixture is given by ASTM D6484 as shown in Figure 2.3 [10]. The wide sections grip the coupon while the middle section of the assembled fixture prevents buckling. The Boeing

Company reaffirmed in 2003 that with a notch in the middle of the specimen, failure happens in the ungripped middle portion [11].

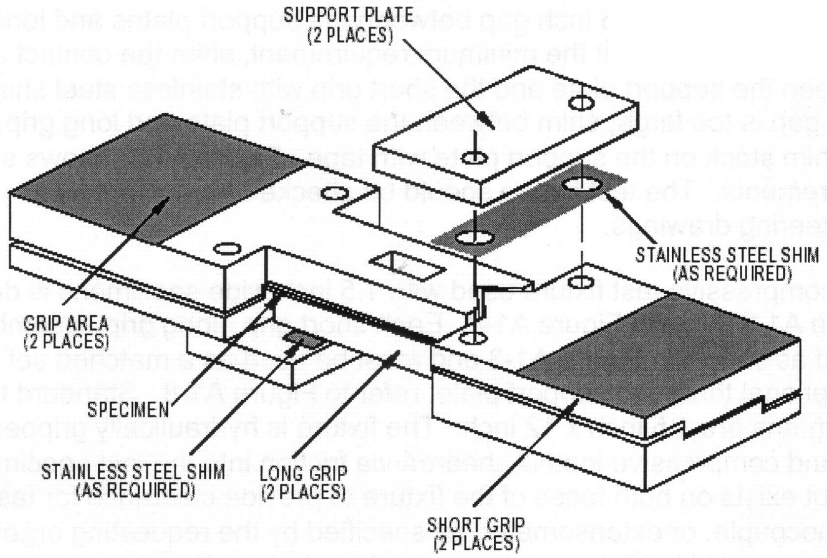

Figure 2.3 Boeing Spec. BSS 7260 OHC Fixture

2.1.3 Overlapping Items of Discussion

This section will cover topics related to both tension and compression fatigue.

2.1.3.1 Fatigue Damage Periods

During cyclic loading, B. Turcic [12] observed three periods of damage growth in fibrous composite laminates. These periods have been labeled the incubation period, the stabilized damage period, and the final period of progressive damage [12]. These periods are easily separated on a graph of compliance (or stiffness) versus number of cycles as seen in the Figure 2.4.

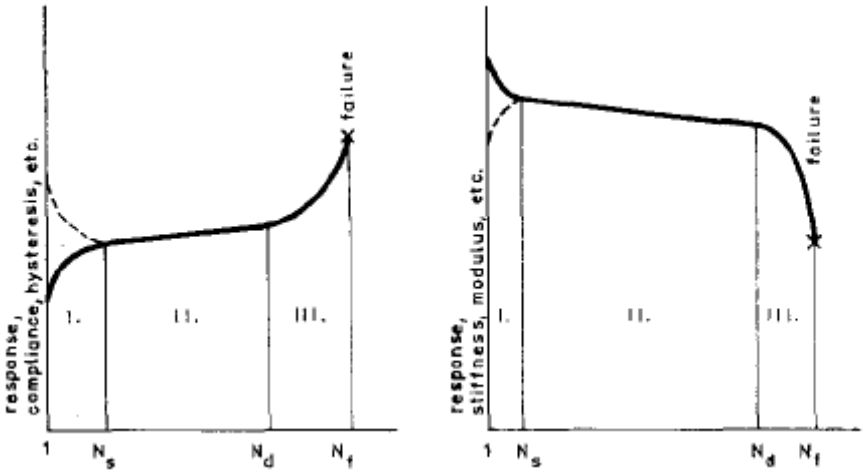

Figure 2.4 Fatigue Damage Periods during cyclic loading

To develop these curves, a T300-914 carbon-epoxy system with a $[0/\pm45/90]_{2s}$ layup was used in a 240x26mm notched composite specimen with a 6mm hole, under load control. Table 2.1 is a sample data set displaying the dependence of the fatigue periods on the cyclic stress.

Table 2.1: Transitions Between Fatigue Damage Periods

Specimen	*Cyclic stress σ* (MPa)	*Fatigue period limits*			
		Period I	*Period II*		*Period III*
			N_s (cycles)	N_d (cycles)	N_f (cycles)
3/9	397	0	700	2000	—
24/1	368	0	60000	368000	425600
24/2	368	0	65000	297000	—
24/3	368	0	95000	220600	738730
24/4	407	0	15500	26000	37220
24/5	407	0	75000	170000	233800
24/9	426	0	500	500	920
24/10	426	0	20	20	40
25/1	426	0	1100	1100	2540
25/3	426	0	3900	3900	6380
25/7	397	0	90000	165000	399020
25/8	397	0	44000	75000	87990
25/9	397	0	17000	40000	55810
25/10	368	0	190000	330000	498760
156/1	368	0	65000	241000	742900
156/2	378	0	72000	625000	768510
156/3	378	0	77000	595000	713570
156/4	378	0	74000	172000	439440
156/5	378	0	39000	387000	543540
156/6	387	0	70000	220000	—
156/8	387	0	510	900	1780
272/11	410	0	7000	17570	—
272/12	370	0	7000	94000	—
273/11	410	0	5500	13000	27510
273/12	370	0	16000	114000	234540
274/11	370	0	18000	70000	—

—, failure.

One conclusion from this data is that the transition points between periods (N_s, N_d, and N_f) are dependent on each other and independent of the cyclic loading level. These curves are easily modeled in logarithmic coordinates using power functions [12].

2.1.3.2 Notch Sensitivity

The notch in a composite laminate responds differently depending on the stress ratio encountered during fatigue, as seen by G. Maier in 1987 [13]. Work done with carbon fiber reinforced polyimides revealed interesting behavior at stress ratios (R) = 0.1 and -1.

For R=0.1, the specimen did not completely fail before 2 million cycles, so long as the maximum fatigue stress did not exceed the static tensile strength of the composite. For R=-1, the influence of the notch decreased with increasing cycles. The Figure 2.5 shows an x-ray of a specimen tested to static failure, and one tested at R=-1 near its compressive maximum stress.

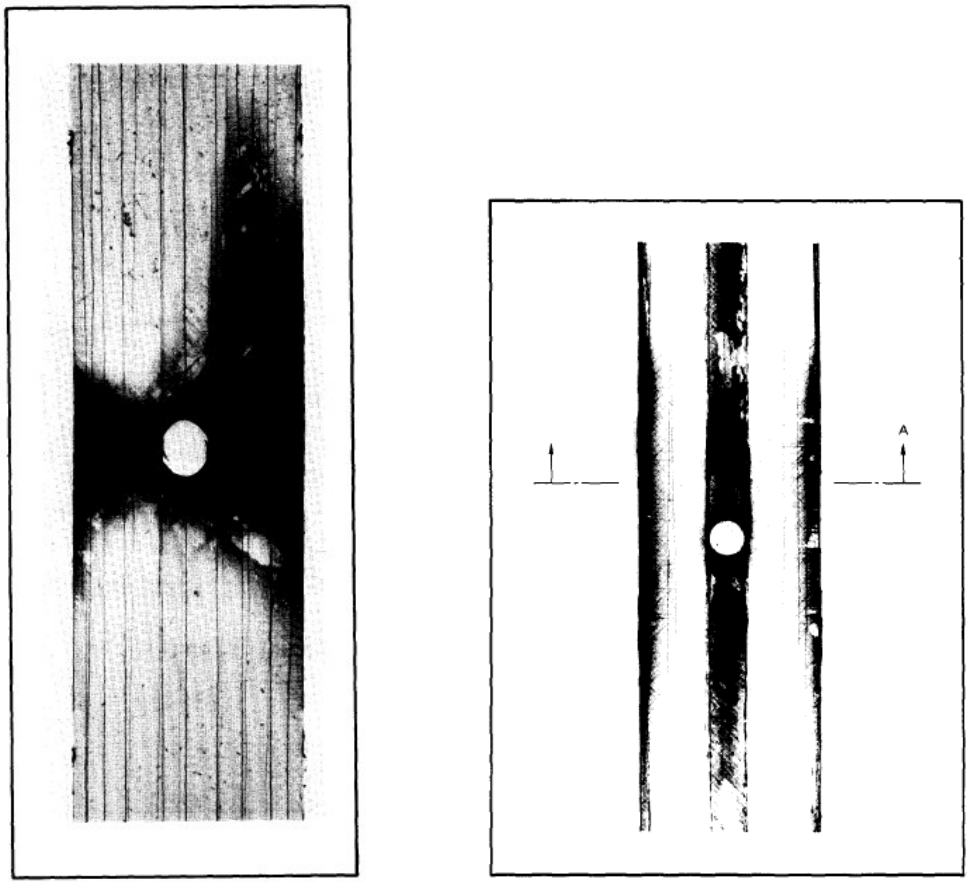

Figure 2.5 Notch Sensitivity at Different Stress Ratios

The different damage mechanisms in compression, as compared with static or tensile fatigue, are the driving force behind the decreasing influence of the notch. Fiber splitting, as opposed to fiber breakage or matrix cracking, extends significantly away from the hole. As these splits increase, the material begins to behave as two separate columns, with the material directly above and below the hole not carrying much of the

load. This fiber splitting obstructs shear transfer around the hole [13]. These specimens also confirmed the existence of fatigue periods, as discussed earlier, with specific damage developments characterizing the regions of the stiffness – cycle curve.

2.2: Modeling Approach

Obtaining data for input into models of predictive relationships is the goal of this test project. Ideal models would include relationships between the fatigue damage observed in a notched composite laminate, including the damage mechanism and the extent of the damage, and the residual stiffness and strength of the laminate. For simple composites, such as unidirectional and unnotched specimens, predicting tensile strength can be achieved through a rule of mixtures. However, this method simplifies the analysis by assuming a particular value for the stiffness of the fiber, rather than a typical range of values – which is common in a manufacturing scenario. Multiple theories exist for obtaining other properties of the lamina, such as transverse stiffness or Poisson's ratio. These include theories by Voight [14], Reuss [15], Hashin [16], Chamis [17], Halpin-Tsai [18], and Mori-Tanaka [19]. Compressive strength can be found using an energy method to acquire buckling equations. To accommodate typical layups that are not unidirectional (but maintaining the unnotched assumption), various failure theories have evolved to handle the different lamina orientations and interactions. These include Maximum Stress [20], Tsai-Wu [21], and Hashin [16].

Deviating from unnotched specimens requires increasingly intensive solutions that are very layup-specific. Further, different models may be necessary for predicting matrix crack growth as well as delaminations in the laminate. For finding the notched strength of a composite under static loading, the Waddoups, Eisenmann, and Kaminski

Failure Theory used existing linear elastic fracture mechanics methodologies previously only employed for characterizing metals, and they found limited success when applied to composites in 1971 [22]. Cruse continued this work, and an outline of his research will be explained. The Whitney-Nuismer Failure Theory in 1974 used the unnotched strength of the composite and a "characteristic distance", an experimental constant, to predict the notched strength [23]. Various research has built upon this last theory, with the nuances between them being the relationship between the characteristic distance and the radius of the notch. One improvement, by Karlak in 1977, is the added dependence on the stacking sequence in the composite, further mimicking the true behavior of the notched specimen [24].

2.2.1 Cruse's Extension of LEFM to Composites

T.A. Cruse, in 1972, extended the ideas behind linear elastic fracture mechanics that were developed for metals to composite materials in an attempt to explain the complicated fractures witnessed [25]. By finding the apparent fracture toughness for composite materials experimentally, the homogeneous continuum model that LEFM was based on appeared valid. He used three-point bending specimens to calculate strain energy release rates for fractures across fibers and for those between fibers. The three-point bending specimens were end-notched with varying initial crack lengths; an example of which is shown in Figure 2.6.

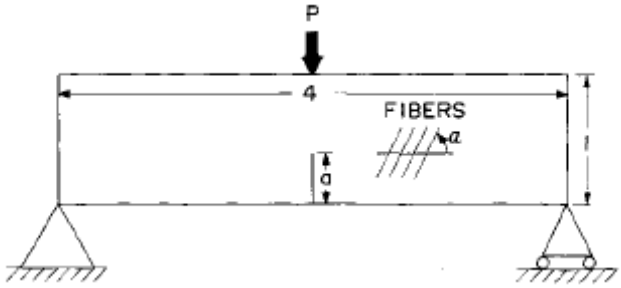

Figure 2.6 Notched Specimens for Three-Point Bending

The stress intensity factors that corresponded to each test established a material parameter that characterized the composite laminate as a homogeneous system. For comparisons between different laminates, the stress intensity factors were split into their Mode I (crack opening) and Mode II (in-plane shear) components. Using a finite element solution to calculate σ_y and τ_{xy} at the crack tip, the authors determined the strain energy release rate for collinear crack growth as well as Rice's J-integral [26].

2.2.2 Damage Growth Model

Until now, these theories mainly address static strength. To determine fatigue strength of notched composites, various models have been introduced to attempt to predict such complex behavior of a composite system under fatigue loading.

The damage growth model, as put forth by S.M. Spearing in 1984, begins with the Paris Law, in which $\frac{da}{dN} = \lambda_1(\Delta K)^m$, where da/dN is the crack growth rate, ΔK is the stress intensity factor, and λ_1 and m are constants [27]. Using the split growth rate, dl/dN, and energy release rate G, $\frac{dl}{dN} = \lambda_2(\Delta G)^{m/2}$, with λ_2 being a different constant.

Past research has attempted to use a similar power law to describe edge delamination growth. Describing the damage at the notch tip involves including both splits and delaminations, which is not possible using either of these equations. Since delamination is dependent on the square of the split, the current toughness G must be used to normalize ΔG. This results in $\frac{dl}{dN} = \lambda_3 \left[\frac{\Delta G}{G_c}\right]^{m/2}$, λ_3 being a different constant again. Figure 2.7 shows the geometry of the damage around a notch in a cross-ply laminate.

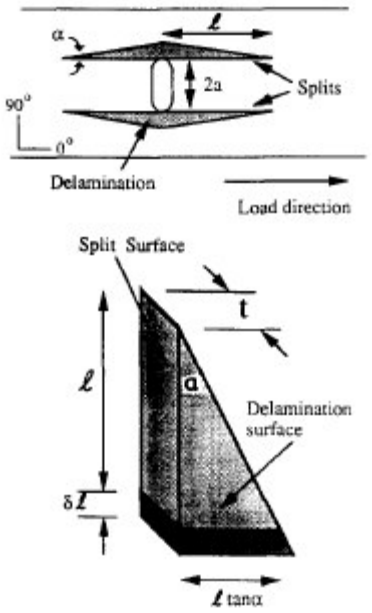

Figure 2.7 Geometry for Damage Growth Model

A large amount of research has been performed concerning modeling of various layups consisting only of 0°, 45°, and 90° plies. Beginning with $(90/0)_s$ laminates, one of the simplest cases, an energy balance of one quarter of the specimen (half the width and half the thickness) leads to $\delta E_{ab} = G_s t\, \delta l + G_d(l \tan \alpha)\, \delta l$, where δE_{ab} is the energy absorbed from the new crack surfaces, G_s is energy absorbed per unit of split, G_d is energy absorbed per unit of delamination, t is the thickness, and α is the delamination angle. The

total energy of the system decreases crack or split extension, increasing compliance.

Given by the relation $\delta E_r = \frac{1}{2} P^2 \, \delta C$, where P is one quarter of the applied load and δC is the change in compliance, damage criteria can be established as $\delta E_r \geq \delta E_{ab}$ for the damage to continue to increase in size. When $E_r = E_{ab}$, $\frac{P^2}{2t}\frac{\partial C}{\partial l} = G_s + G_d \frac{l \tan \alpha}{t}$, this gives the split initiation load as $P_i = \left[\frac{2G_s t}{\frac{\partial C}{\partial l}\Big|_{l=0}} \right]^{1/2}$. Continued growth is modeled by $l = \frac{P^2 \left(\frac{\partial C}{\partial l}\right)}{2G_d \tan \alpha} - \frac{G_s}{G_d}\left[\frac{t}{\tan \alpha}\right]$. Since $\frac{\partial C}{\partial l}$ is difficult to analytically determine, a finite element solution was employed to numerically approximate it. As seen in Figure 2.8, the model accurately predicts the split length for different thickness specimens [27].

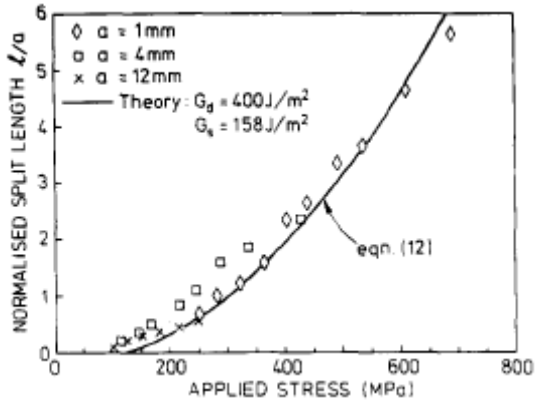

Figure 2.8 Damage Growth Model Accuracy with Different Thicknesses

Using a similar approach, an equation for split length as a function of number of cycles can be obtained by integrating $\frac{dl}{dN} = \lambda \left[\frac{1/2(\Delta P)^2 \left(\frac{\partial C}{\partial l}\right)}{G_s t + G_d l \tan \alpha} \right]^{m/2}$ and arriving at the following

equation: $$l = \frac{1}{G_d \tan\alpha}\left[\lambda(\Delta G)^{m/2}\left[\frac{m+2}{2}\right] \times (G_d \tan\alpha)N + (G_s t + G_d l_0 \tan\alpha)^{(m+2)/2}\right]^{2/(m+2)}$$.

Validating this model with different far-field stresses is shown in Figure 2.9.

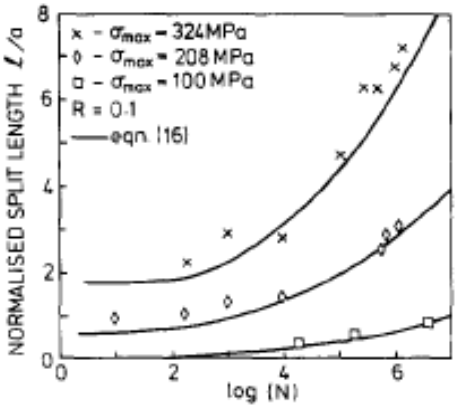

Figure 2.9 Damage Growth Model Accuracy at Different Cycles

For R=0.1, the split lengths follow those predicted (bold lines) from the above equation.

Spearing continues with other laminate variations of 0° and 90° plies, such as $(90_i/0_j)_{ns}$, $(90_i/0_j)_s$, and $(90/0)_{ns}$, eventually progressing to $(90/+45/-45/0)_s$. In all cases, the dominant modes (splitting, delamination, etc.), and locations (between specific plies or longitudinal splits as opposed to transverse cracking), of damage were known. For the $(90/+45/-45/0)_s$ laminate, the author regarded splitting in the 0° plies and delamination between the 0° ply and the -45° ply as the controlling mode of failure. In this case, $\delta E_{ab} = G_s t\,\delta l + G_d \frac{(l+k)}{2}\delta l$, with k relating the delamination to the notch as seen in Figure 2.10.

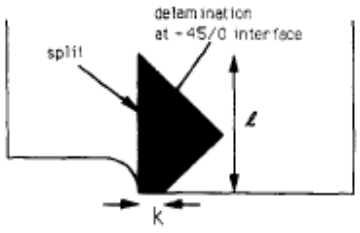

Figure 2.10 Delamination at Notch Interface

Acquiring $\frac{\partial C}{\partial l}$ from a finite element solution, and using the equation for split length as $l = \frac{P^2}{G_d}\frac{\partial C}{\partial l} - \frac{2G_s t}{G_d} - k$, split lengths as a function of stress are determined. This is shown in Figure 2.11.

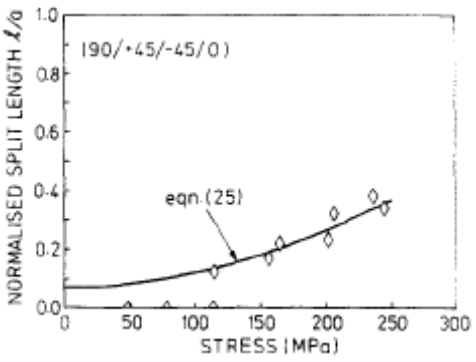

Figure 2.11 Split Length as a Function of Stress

For split lengths in fatigue, the relations derived earlier for $(90/0)_s$ yield

$$\frac{dl}{dN} = \lambda \left[\frac{1/2(\Delta P)^2 \left(\frac{\partial C}{\partial l}\right)}{G_s t + G_d \left(\frac{l+k}{2}\right)} \right]^{m/2}$$

, with the appropriate constants. Plotting the split length as a function of cycles displays accurate results, as shown in Figure 2.12.

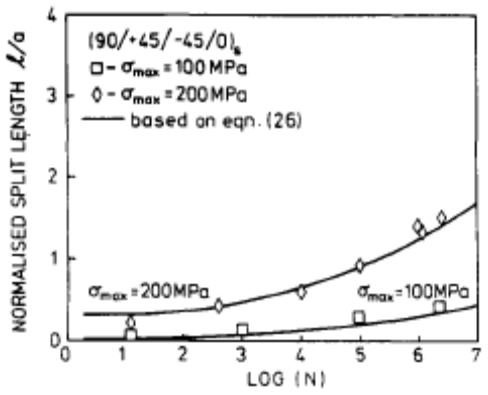

Figure 2.12 Split Length as a Function of Cycles

The conclusions drawn from this fatigue modeling were that, given an idea of the damage pattern around a notch, from past experimentation, the extent of damage could be predicted based on loading and cycles [27]. The actual path of damage is not predicted, and residual stresses and transverse ply cracks are not calculated.

2.2.3 Progressive Fatigue Damage Modeling

The progressive fatigue damage model, explained by M. Shokrieh in 2000, handles both notched and unnotched composite laminates through the use of stress analysis, failure analysis, and material property degradation rules. The goal of this model was to create one which could handle any geometry, lay-up, loading, stress ratio, or boundary condition. Using progressive damage modeling, damage progression has been studied extensively in static loading, and now is being extended to fatigue [28]. The example used to test this model involved a pin/bolt-loaded composite plate; the complexity of the experiment would test the model's accuracy at predicting residual strength and life, direction of failure propagation, and final fatigue life of the composite

specimen. The flowchart in Figure 2.13 explains the methodology behind this process [26, 27].

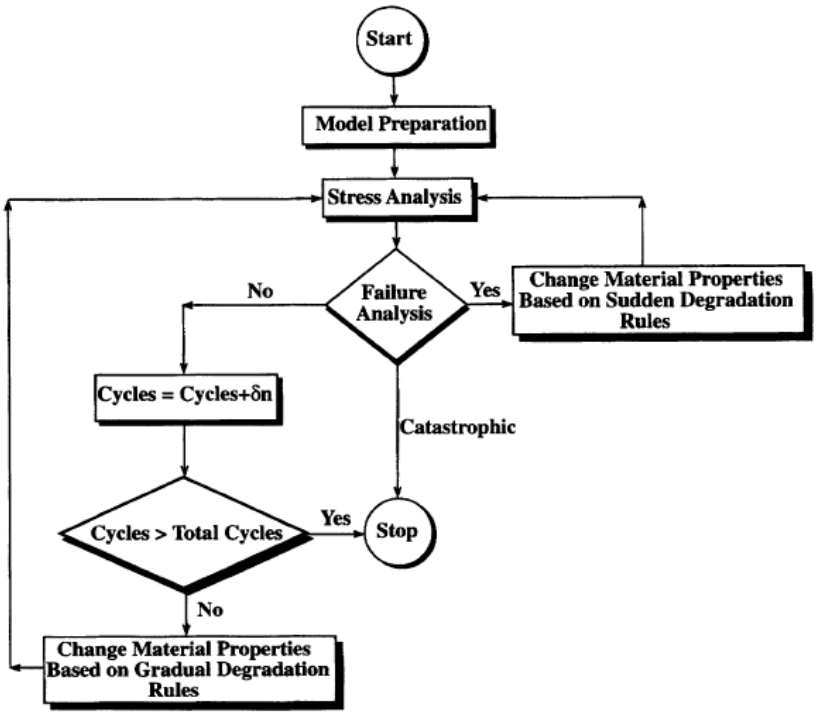

Figure 2.13 Progressive Fatigue Damage Model Flowchart

To simplify the stress analysis, only cross-ply and angle-ply laminates were used in this experiment (such as $[0_4/90_4]_s$, $[90_4/0_4]_s$, and $[+45_4/-45_4]_s$). Increasing the number of elements, near the hole and near the edge in order to account for delamination, enables the model to capture the failure initiation resulting from the stress concentrations and boundary conditions.

After the stress analysis is finished for the given specimen's geometry and current material properties, failure analysis is performed, with seven different possible failure modes examined. These modes are fiber tension, fiber compression, fiber-matrix

shearing, matrix tension, matrix compression, normal tension and normal compression failure modes. Analysis is performed on a ply-by-ply basis, with each ply treated as a unidirectional ply under a multiaxial state of stress. For each possible mode of failure, a failure criterion is applied to the specimen to determine if there should be a sudden or gradual degradation of material properties [28, 29].

For the criterion used to evaluate the first mode of failure, fiber tension fatigue is given by the equation:

$$\left(\frac{\sigma_{xx}}{X_t(n,\sigma,\kappa)}\right)^2 + \left(\frac{\dfrac{\sigma_{xy}^2}{2E_{xy}(n,\sigma,\kappa)} + \dfrac{3}{4}\delta\sigma_{xy}^4}{\dfrac{S_{xy}^2(n,\sigma,\kappa)}{2E_{xy}(n,\sigma,\kappa)} + \dfrac{3}{4}\delta S_{xy}^4(n,\sigma,\kappa)}\right)$$

$$+ \left(\frac{\dfrac{\sigma_{xz}^2}{2E_{xz}(n,\sigma,\kappa)} + \dfrac{3}{4}\delta\sigma_{xz}^4}{\dfrac{S_{xz}^2(n,\sigma,\kappa)}{2E_{xz}(n,\sigma,\kappa)} + \dfrac{3}{4}\delta S_{xz}^4(n,\sigma,\kappa)}\right) = g_{F+}^2 \quad (\text{if } g_{F+} > 1, \text{ then failure})$$

In this case, X_t (n, σ, K) represents the longitudinal tensile residual fatigue strength under uniaxial loading, S_{xy} (n, σ, K) represents the in-plane residual shear fatigue strength of a unidirectional ply under uniaxial shear fatigue loading, E_{xy} (n, σ, K) is the in-plane residual fatigue shear stiffness, and S_{xz} (n, σ, K) and E_{xz} (n, σ, K) represent the out-of-plane shear strength and stiffness. The remaining variables n, σ, K, and δ are the number of cycles, stress, stress ratio, and material nonlinearity parameter (assumed a constant value throughout fatigue). The equation emphasizes the dependence of the strength and stiffness values as a function of n, σ, K; if they were not, the equation would simplify to a three-dimensional static failure criterion.

The second mode of failure, fiber compression fatigue, is modeled by the following equation where X_c is the longitudinal compressive residual fatigue strength for a unidirectional ply experiencing uniaxial fatigue.

$$\left(\frac{\sigma_{xx}}{X_c(n,\sigma,\kappa)}\right) = g_{F^-} \qquad (\text{if } g_{F^-} > 1, \text{ then failure})$$

One note is the lack of shear stresses interacting with the compressive behavior.

The third failure mode, fiber-matrix shearing fatigue failure, when applied to a unidirectional ply under multiaxial loading is given by the following equation.

$$\left(\frac{\sigma_{xx}}{X_c(n,\sigma,\kappa)}\right)^2 + \left(\frac{\dfrac{\sigma_{xy}^2}{2E_{xy}(n,\sigma,\kappa)} + \dfrac{3}{4}\delta\sigma_{xy}^4}{\dfrac{S_{xy}^2(n,\sigma,\kappa)}{2E_{xy}(n,\sigma,\kappa)} + \dfrac{3}{4}\delta S_{xy}^4(n,\sigma,\kappa)}\right) + \left(\frac{\dfrac{\sigma_{xz}^2}{2E_{xz}(n,\sigma,\kappa)} + \dfrac{3}{4}\delta\sigma_{xz}^4}{\dfrac{S_{xz}^2(n,\sigma,\kappa)}{2E_{xz}(n,\sigma,\kappa)} + \dfrac{3}{4}\delta S_{xz}^4(n,\sigma,\kappa)}\right) = g_{FM}^2$$

$$(\text{if } g_{FM} > 1, \text{ then failure})$$

The fourth mode is matrix tension fatigue failure, shown in the following equation.

$$\left(\frac{\sigma_{yy}}{Y_t(n,\sigma,\kappa)}\right)^2 + \left(\frac{\dfrac{\sigma_{xy}^2}{2E_{xy}(n,\sigma,\kappa)} + \dfrac{3}{4}\delta\sigma_{xy}^4}{\dfrac{S_{xy}^2(n,\sigma,\kappa)}{2E_{xy}(n,\sigma,\kappa)} + \dfrac{3}{4}\delta S_{xy}^4(n,\sigma,\kappa)}\right) + \left(\frac{\sigma_{yz}}{S_{yz}(n,\sigma,\kappa)}\right)^2 + g_{M^+}^2$$

$$(\text{if } g_{M^+} > 1, \text{ then failure})$$

Y_t (n, σ, K) represents the transverse tensile residual fatigue strength, with S_{yz} (n, σ, K) being the out-of-plane shear residual strength.

Matrix compression fatigue failure occurs in the model when the following condition is met. Y_c (n, σ, K) represents the transverse compressive residual fatigue strength.

$$\left(\frac{\sigma_{yy}}{Y_c(n,\sigma,\kappa)}\right)^2+\left(\frac{\frac{\sigma_{xy}^2}{2E_{xy}(n,\sigma,\kappa)}+\frac{3}{4}\delta\sigma_{xy}^4}{\frac{S_{xy}^2(n,\sigma,\kappa)}{2E_{xy}(n,\sigma,\kappa)}+\frac{3}{4}\delta S_{xy}^4(n,\sigma,\kappa)}\right)+\left(\frac{\sigma_{yz}}{S_{yz}(n,\sigma,\kappa)}\right)^2+g_{M^-}^2$$

(if g_{M^-} >1, then failure)

Normal tension fatigue failure is due to through-thickness tensile stresses in a ply.

$$\left(\frac{\sigma_{zz}}{Z_t(n,\sigma,\kappa)}\right)^2+\left(\frac{\frac{\sigma_{xz}^2}{2E_{xz}(n,\sigma,\kappa)}+\frac{3}{4}\delta\sigma_{xz}^4}{\frac{S_{xz}^2(n,\sigma,\kappa)}{2E_{xz}(n,\sigma,\kappa)}+\frac{3}{4}\delta S_{xz}^4(n,\sigma,\kappa)}\right)+\left(\frac{\sigma_{yz}}{S_{yz}(n,\sigma,\kappa)}\right)^2+g_{N^+}^2$$

(if g_{N^+} >1, then failure)

Normal compression fatigue failure is the last mode examined in the failure analysis, using the following equation.

$$\left(\frac{\sigma_{zz}}{Z_c(n,\sigma,\kappa)}\right)^2+\left(\frac{\frac{\sigma_{xz}^2}{2E_{xz}(n,\sigma,\kappa)}+\frac{3}{4}\delta\sigma_{xz}^4}{\frac{S_{xz}^2(n,\sigma,\kappa)}{2E_{xz}(n,\sigma,\kappa)}+\frac{3}{4}\delta S_{xz}^4(n,\sigma,\kappa)}\right)+\left(\frac{\sigma_{yz}}{S_{yz}(n,\sigma,\kappa)}\right)^2+g_{N^-}^2$$

(if g_{N^-} >1, then failure)

Material property degradation follows the results of the failure analysis. The method of progressive fatigue damage modeling degrades the set of ply properties according to what type of failure they experience, if any. If failure occurs, it is labeled as "sudden degradation" in the flowchart. If no failure occurs, gradual degradation occurs and the

specimen is cycled again. The only catastrophic failure is fiber tension or fiber compression failure. In that case, all properties are degraded to zero as follows.

If the laminate plies pass the stress analysis and failure analysis without sudden or catastrophic damage, the cycle count is increased and gradual degradation of the plies occurs. In this case, residual strength and stiffness and fatigue life are calculated according to equations taken from work by T. Adam in 1986 [30] when applied to arbitrarily oriented uniaxially loaded ply. The residual strength is obtained by

$$R(n,\sigma,\kappa)=\left[1-\left(\frac{\log(n)-\log(.25)}{\log(N_f)-\log(.25)}\right)^{\beta}\right]^{1/\alpha}(R_s-\sigma)+\sigma$$

in which

$R(n,\sigma,\kappa)$ = residual strength
R_s = static strength
n = number of applied cycles
σ = magnitude of applied maximum stress
N_f = fatigue life at σ
κ = stress ratio
α and β = experimental curve fitting parameters

Similarly the stiffness is found from

$$E(n,\sigma,\kappa)=\left[1-\left(\frac{\log(n)-\log(.25)}{\log(N_f)-\log(.25)}\right)^{\lambda}\right]^{1/\gamma}\left(E_s-\frac{\sigma}{\varepsilon_f}\right)+\frac{\sigma}{\varepsilon_f}$$

where

$E(n,\sigma,\kappa)$ = residual stiffness
E_s = static stiffness
ε_f = average strain to failure
γ and λ = experimental curve fitting parameters

The normalized fatigue life for this unidirectional ply is given by

$$u=\frac{\ln(a/f)}{\ln[1-q)(c+q)]}=A+B\log N_f$$ where

f and u = curve fitting parameters
$\sigma_a = (\sigma_{max} - \sigma_{min})/2$ = alternating stress
$\sigma_m = (\sigma_{max} + \sigma_{min})/2$ = mean stress
$q = \sigma_m/\sigma_t$
$a = \sigma_a/\sigma_t$
$c = \sigma_c/\sigma_t$
σ_t = tensile strength
σ_c = compressive strength

The desired benefit of this progressive model is the simplification of the test matrix required to determine fatigue properties across a wide range of loads and stress ratios. Finding two curve-fitting constants in each equation is quicker than creating extensive data sets and fitting polynomial failure criteria, which have limited applications. Modeling the geometry and determining on-axis stresses leads to performing failure analysis and checking for sudden or catastrophic material property degradation [29].

2.2.4 "Natural" Fatigue Damage Cumulation vs. Palmgren-Miner

The "Natural" Fatigue Damage Cumulation Model, when applied to composite laminates, predicts fatigue life approximately an order of magnitude better than the Palmgren-Miner linear model, as shown by B. Turcic [31]. As with other models, the idea is to predict the damage state against the number of cycles. Due to difficulty directly measuring the damage in the composite, a different parameter has to be used. A mechanical property, such as compliance or hysteresis, may be used to quantify the damage. Likewise, a morphological or physical property may be used, like the area of delamination and crack density or temperature and damping properties of the specimen. The response of the specimen to acoustic or electron or positive ion emission also can correlate to the actual damage in the specimen.

Revisiting the discussion about fatigue periods, there are three periods of fatigue: incubation damage, stabilized damage, and progressive failure. Past research has shown that the damage state at the end of fatigue Period I is independent of the loading level, most notably by Reifsneider and his "characteristic damage state." This set amount of damage, found at the end of Period I, suggests that a similar damage state might exist between Periods II and III – the periods of linear damage progression and final failure. The model assumes logarithmic increase in damage for Period I, linear behavior for Period II, and exponential increase during Period III [31].

Breaking up the model into a piecewise function allows boundary conditions, and compatibility at transitions between periods, to dictate a damage parameter equation D(N) as a function of the number of cycles. Using N_s and N_d as the cycle counts after Period I and Period II, and α, β, δ, and ɣ as constants, the conditions are

$$\begin{array}{lll} D(0)=0 & D(N_s)=0 & D(N_d)=0 \\ D(N)=\alpha \ln(N+1) & D(N)=\beta(N-N_s) & D(N)=\gamma[\exp\{\delta(N-N_d)\}-1] \\ D(N_s)=1 & D(N_d)=1 & D(N_f)=1 \end{array}$$

for the three periods. For a continuous function between the periods, $\alpha=\frac{1}{\ln(N_s+1)}$,

$\beta=\frac{1}{(N_d-N_s)}$, $\delta=\frac{\ln\{1+\alpha/(N_s+1)\delta\}-\ln\{\alpha/(N_s+1)\delta\}}{N_f-N_d}$, and $\gamma=\frac{\alpha}{(N_s+1)\delta}$.

Using carbon-epoxy quasi-isotropic laminates with a central notch, two-load-level fatigue schemes were placed on the specimens. Combinations of the fatigue levels were used to help isolate the damage states characteristic of the transitions between the fatigue periods. This is shown in Figure 2.14.

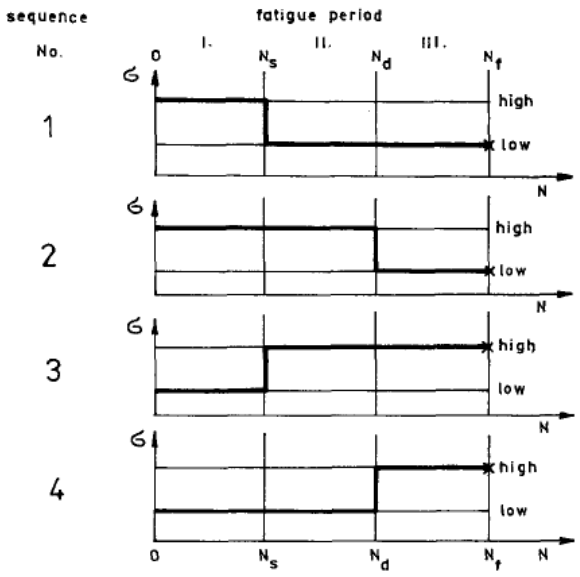

Figure 2.14 Fatigue Schemes Used to Isolate Transition Points

A high load level, 90% of the ultimate strength, and a lower fatigue level, 78% of ultimate strength, were applied as the experimental loads to test the "natural" cumulation model for accuracy and compare its results with those obtained from the Palmgren-Miner linear rule. Cyclic tension was also chosen for testing, with a stress ratio R = 0.05 at a frequency of 10 Hz. Due to non-linear behavior from complex damage modes, typical of non-unidirectional composites, the Palmgren-Miner linear model should provide inferior accuracy compared to the natural model.

Comparing the two models yields surprisingly different results when compared to actual testing. This comparison is shown in Table 2.2.

Table 2.2: Predictions of Transitions Between Fatigue Damage Periods

Specimen	*Block sequence type*	*Palmgren-Miner model*		*"natural" model*	
		N_f'/N_f	$(N_f'-N_f)/N_f$	N_f'/N_f	$(N_f'-N_f)/N_f$
Stacking sequence of $(0/\pm 45/90)_{2s}$					
271/11	1	7.129	−0.8938	0.9964	-3.559×10^{-3}
271/12	1	4.935	−0.9265	0.7691	−0.2309
272/11	2	1.902	−0.9717	0.9429	−0.05713
272/12	4	0.09828	5.598	0.9267	−0.07329
274/11	4	0.07412	3.976	0.8774	−0.1226
274/12	3	0.02689	0.8053	0.4801	−0.5199
275/11	3	0.1352	8.080	1.961	0.9609
275/12	2	1.401	−0.9791	1.062	0.06216
Stacking sequence of $(90/\pm 45/0)_{2s}$					
271/2	2	1.850	−0.9470	0.6808	−0.3192
272/6	1	6.847	−0.8038	1.457	0.4568
273/8	1	2.396	−0.9313	0.9064	0.09361

The table shows the ratio of predicted fatigue life N_f` over the actual fatigue life. As evident from the table, the "natural" model is usually an order of magnitude better at predicting fatigue life for quasi-isotropic layups. While doubts exist concerning the effects of the mean stress and loading frequency on the model, further testing might validate the model for these other loading conditions. Knowing the "characteristic damage states" at the ends of Fatigue Periods I and II for other layups would enable one to predict the damage parameter values for any cycle. Correlating the parameter value to actual damage would provide information on the extent of damage throughout the fatigue life of the specimen [31].

2.2.5 The Critical Element Model

The critical element model, by K.L. Reifsnider [32], predicts fatigue life and residual strength of a composite through the use of micro-mechanical analysis and understanding failure in "critical elements". Constituents of a composite laminate are divided into "critical" and "subcritical" components, with failure in "critical" ones

leading to overall failure of the composite and failure in the "subcritical" ones rearranging the stress distribution throughout the laminate. One relevant example would be a composite coupon under tensile fatigue loading. The critical elements are the longitudinal, load-bearing plies, while the subcritical ones are the remaining layers. For fatigue loading, the splitting seen along the longitudinal plies is necessarily subcritical damage, due to the laminate's ability to withstand further loading. The following flowchart in Figure 2.15 describes the process used to describe and analyze failure, as well as predict future properties of the laminate:

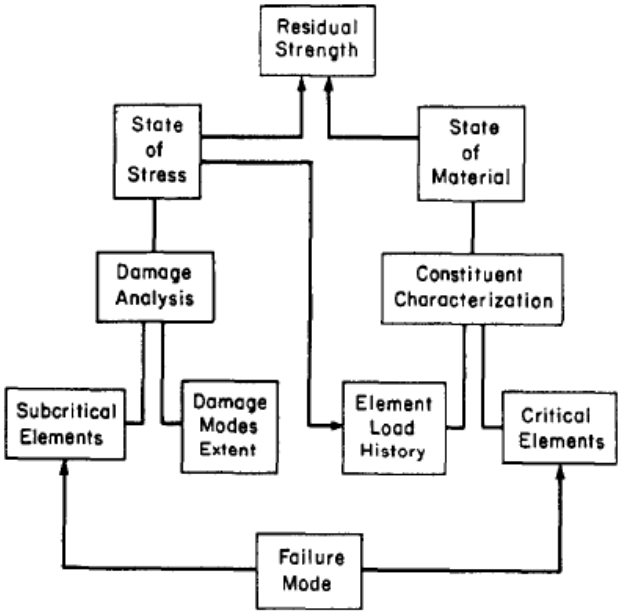

Figure 2.15 Critical Element Flowchart

After splitting the laminate into critical and subcritical parts, damage analysis or characterization can be performed. The properties of the critical elements change (strength, stiffness, etc.) because of the damage in the subcritical elements. From a

macroscopic viewpoint, delaminations and cracks in the matrix change the stress distribution in the critical elements and can locally cause changes in the stress concentration factors. In addition, through the use of continuum damage mechanics, the effects of long-term loading on the critical elements are considered; and they further contribute to the degradation of the load-bearing constituents. It is this macro and micro-level approach that attempts to fully capture the effects of fatigue loading and define the material state while predicting the residual strength of the composite [32].

The advantage to choosing the critical element model is apparent after realizing the number of damage modes in a composite. Numbering in the hundreds, only a fraction of these damages are characterized as failure modes. Limiting the number of damage modes (and corresponding critical elements) significantly reduces the modeling process and expedites the testing required to support the model.

The application of the critical element model is governed by numerous parameters. One important parameter is the stress state the composite experiences. A large percentage of fatigue research deals with one dimensional stress that does not encapsulate the behavior of the material. Multiaxial stress fields are a result of a mismatch in properties between the fiber and matrix, even under uniaxial stress. These fields impact the true life and strength of the material, and can be a source of error if unaccounted for. A second parameter is the geometry of the specimen in question. The most common feature is often a notch, but other variations can contribute to varying the stresses throughout a specimen. The presence of such a notch is apparent when the residual strength is determined. In such cases, the residual strength will actually improve

due to splitting around the notch alleviating some of the stress concentration around the hole. The following graph in Figure 2.16 offers further insight.

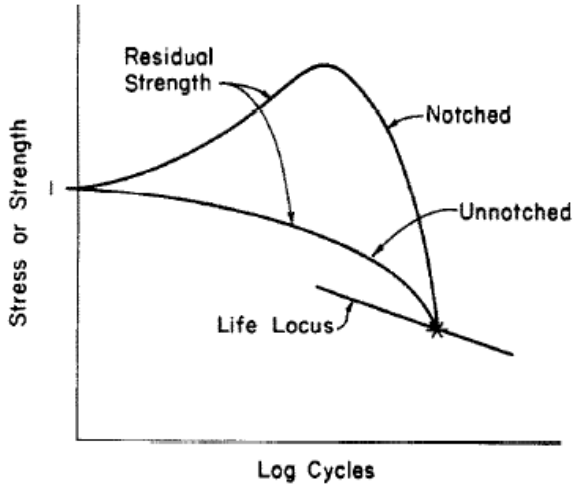

Figure 2.16 Notch Effects on Residual Strength

A third parameter, defined by Reifsnider, is what he called cycle-dependent processes. These processes could include damage accumulation specific to composite systems, and the model should be general enough to accommodate changes as new material systems are introduced. A fourth parameter relates to time-dependent processes. This could include chemical degradation or other environmental effects. A fifth parameter includes statistics concerning the variability of the material properties. Reifsnider did acknowledge that his model did not fully understand the complexity of all the parameters and their interactions, but stated that to assume one could neglect any of them would only lead to a less robust model for design or analysis [32].

Predicting the life of a composite begins with determining the strength after zero cycles for an undamaged critical element, and finding the intersection of a damaged element's strength with the failure state. A qualitative graph is shown in Figure 2.17.

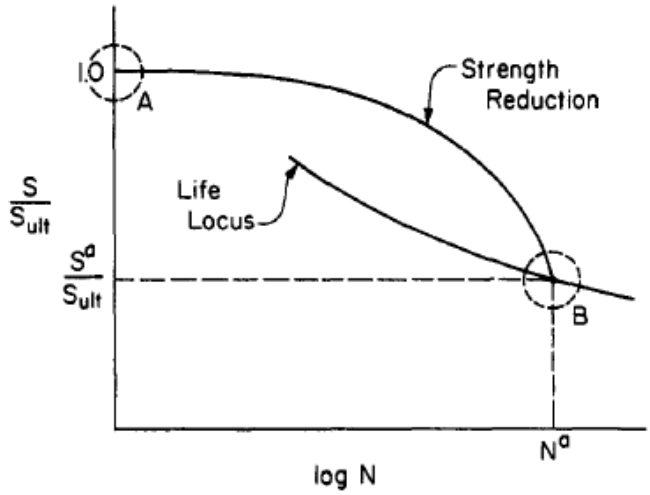

Figure 2.17 Intersection of Damaged Element with Failure State

After setting these two endpoints, careful observation of a property which is proportional to the damage allows interpolation between the points. The change in stiffness could be used. Another option is tracking a dominant crack eventually responsible for failure [32]. Longitudinal cracking of carbon fiber composite laminates will be examined in the proceeding chapters with the intention of building a future model with the data.

Chapter 3 : MATERIAL AND EXPERIMENTAL METHODS

This section will cover the specimens, equipment, and test procedures used as well as a description and justification of the fatigue test plan.

3.1 Specimens

Using a carbon fiber/epoxy prepreg, the specimens were laid up by hand and cured into panels. They were cut with a diamond saw and drilled using a diamond-impregnated drill bit. X-rays were taken of the specimens prior to each test to ensure that there was no damage from manufacturing or shipping. The three layups included were all 20 ply laminates with the following stacking sequences: $[0_4/45/0_3/90/0]_s$, $[45/90/-45/0_2/45/0_2/-45/0]_s$, $[\pm5/65/(\pm5)_2/-65/\pm5]_s$, and $[\pm5/65/(\pm5)_2/-65/5/65]_s$. Hereafter, these laminates will be referred to by the percentage of certain plies. $[0_4/45/0_3/90/0]_s$ and $[45/90/-45/0_2/45/0_2/-45/0]_s$ will be known as 80/10/10 and 50/40/10 – the percentage of 0°/45°/90° plies. $[\pm5/65/(\pm5)_2/-65/\pm5]_s$ becomes 80/20 (80% of ±5° plies, 20% of ±65° plies). $[\pm5/65/(\pm5)_2/-65/5/65]_s$ becomes 70/30 (70% of ±5° plies, 30% of ±65° plies). These laminates are all considered to be "hard" laminates, because the longitudinal stiffness is significantly higher than the transverse stiffness. The specimens were cut into 38.1mm by 304.8mm sections with a 6.35mm hole in the middle of the coupon specimen.

Longitudinal and transverse properties of all the laminates were determined from classical lamination theory after inputting the known ply properties. Using the acquired data, the stress concentrations for the open hole, according to Lekhnitskii [3], were found

from the equation: $K_T^{\infty} = 1 + \left[\left(\frac{E_{11}}{G_{12}} \right)^{1/2} - 2\nu_{12} + 2\left(\frac{E_{11}}{E_{22}} \right)^{1/2} \right]^{1/2}$. For the 50/40/10, the concentration factor was 3.12. For the 70/30 specimens, it was 3.48. Lastly, for the 80/20, it was 3.69.

3.2 Equipment

A 100kN servo-hydraulic test frame was used to fatigue the composite laminates. The residual strength tests were conducted in a similar 500kN test frame. Both units had computer control with data acquisition capability and strain was measured using a 2.54cm extensometer. The x-ray system had a 120kV limit and was set up around the 100kN test frame as shown in Figure 3.1. It also has a 0.5 mm focal spot size, self-rectifying thermionic X-ray tube with a beryllium window, 0.76 mm Beryllium window thickness, and 30 degree beam divergence. For radiation safety, a lead-lined box surrounded the grips and test assembly, as shown in Figure 3.1.

Figure 3.1 X-ray system and test frame

3.3 Procedures

Strength of unnotched laminates was obtained in order to compare the residual strength results and normalize the graphs. Fatigue testing was performed at 5 Hertz. Specimens of each laminate were tested, one each at R = -0.1 (Tension), R = -10 (Compression), R = -1 (Fully Reversed), R = -0.35 (Mostly Tension), and R = -3 (Mostly Compression). An anti-buckling plate surrounded the coupon to prevent large-scale buckling of the coupon under compressive loading. The Teflon-coated anti-buckling plate carried no axial loading during testing, and is shown in the test frame in Figure 3.2. The bolts were tightened to approximately 2.8 N-m (39 in-lbs.).

Figure 3.2 Anti-buckling fixture surrounding coupon in test frame

The x-ray procedure used Polaroid type 55 P/N sheet film with a voltage of 52kV, 3mA amperage, and 73 seconds of exposure. A zinc iodide solution was first applied to the inside surface of the hole and coupon free edges with a syringe. The solution consisted of 60g zinc iodide, 8mL water, 10mL isopropyl alcohol, and 6mL of Kodak PhotoFlow [2]. After waiting 5 minutes to allow the zinc iodide die penetrant to wick

into the any damaged areas, the film was exposed and processed according to the manufacturer's specifications. Digital images were then made from the negative using a stereomicroscope. The negative was backlit, and with a digital camera attached to the microscope, the image was captured. These images typically had a brown tint to them.

Due to the Polaroid film no longer being available in early 2008, the x-ray procedure switched to using Kodak Industrex MX125 13 x 18 cm x-ray film. The process used a voltage of 25kV, 3mA amperage, and 35 seconds of exposure. The film was processed in a dark room, first in a developer for 5 minutes, then a stopper for 30 seconds, then a fixer for 15 minutes, and a rinse for another 15 minutes. As will become evident in the results chapter, the Kodak Industrex film gave higher quality results. The images from the Industrex x-ray film had a grey tint to them and consistently sharp clarity.

3.4: Damage Initiation Concept

This section will describe the fatigue testing procedure, as well as justification why it is an efficient and effective method of comparing laminates across different stresses and cycle counts.

3.4.1 Description

The damage initiation concept involved using an approach to look for stress levels where first detectable damage can be found after 50,000 cycles. Critical damage was arbitrarily defined as 1.27 cm (0.50") under typical inspection methods. If the damage found at a certain stress level did not exceed this criterion, the maximum stress was raised approximately 34.5 MPa (5 KSI), and the specimen was reexamined after another 50,000

cycles at this new higher loading. If the damage, usually longitudinal splitting, exceeded 1.27 cm (0.50”), the test would continue to 1 million cycles to assess long-term damage growth. This concept gleamed the most information from each specimen, as comparisons could be drawn at numerous stress levels and cycle counts. Also, different design methodologies could utilize the information obtained, such as the maximum stress level at which no damage was detected or at what stress level the damage exceeds the defined critical damage.

3.4.2 Damage Verification

Prior to using this “damage initiation method”, preliminary testing was performed at constant stress levels to 1 million cycles. It was noticed that the amount of damage in each specimen mimicked the fatigue damage periods of “incubation” and “stabilization” seen in Section 2.3 [12]. The tests were not sufficiently long enough to see progressive failure. This is shown in Figure 3.3.

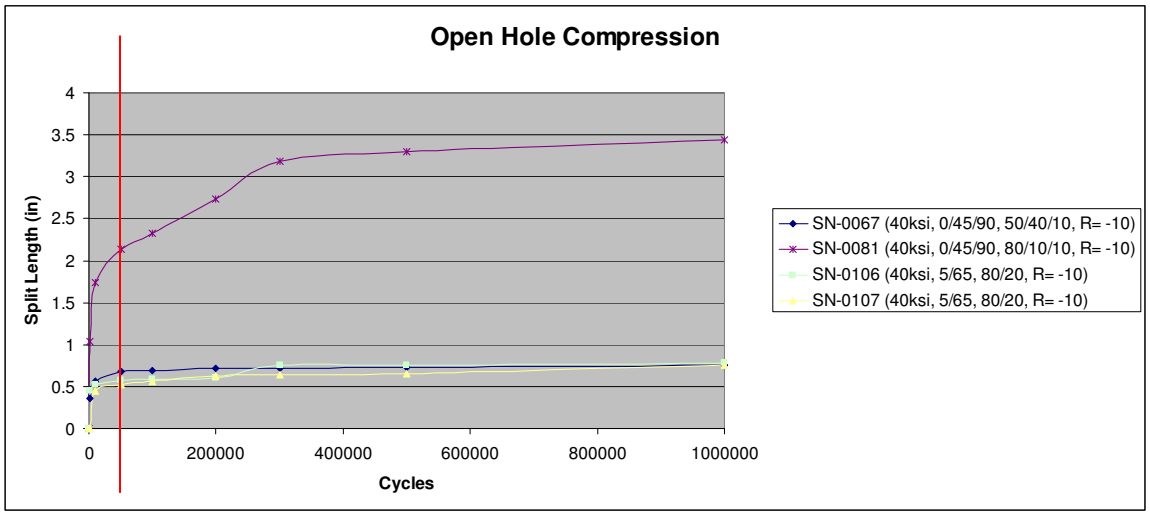

Figure 3.3 Constant Stress Open Hole Compression Tests

Since 60-80% of damage occurs before 50k cycles (compared to damage at 10^6 cycles), this was chosen as an ideal cycle count to determine the effects of each variable. Also, due to excessive damage, the 80/10/10 laminate was not further evaluated. The 80/20 non-traditional laminate has similar stiffness as the 80/10/10, but split lengths in line with the 50/40/10 laminate.

Another possible problem with the test procedure was the effect of removing the fastener at every point to take an x-ray around the hole. Attempts were made to locate damage around the hole without removal of the fastener, but the steel in the bolt head blocked the view of the hole. To determine the effect of constant removal and assembly, two tests were run: one according to the damage initiation method, and another for 1 million cycles at the maximum stress achieved during the first test. A comparison is shown in Figure 3.4.

A) 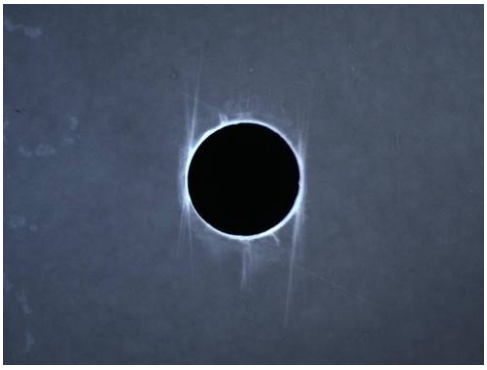 B) 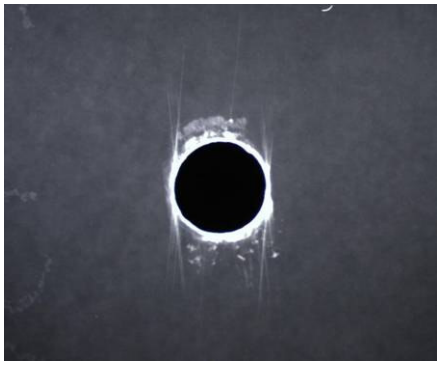

Figure 3.4 Radiographic images around 6.35mm diameter notch after 1 million cycles at max stress in Filled Hole Fully Reversed a) 80/20 laminate run according to Damage Initation Method, b) 80/20 laminate only run at highest stress reached

3.4.3 Sample Series of Data Collected

For each specimen, in-situ x-rays were taken at each stopping point in the test procedure. For the following specimen, an x-ray was taken of the new specimen, as well as after each of the four stress levels it cycled at for 50k cycles, as well as after completing 1 million cycles at the highest stress reached. This is shown in Figure 3.5.

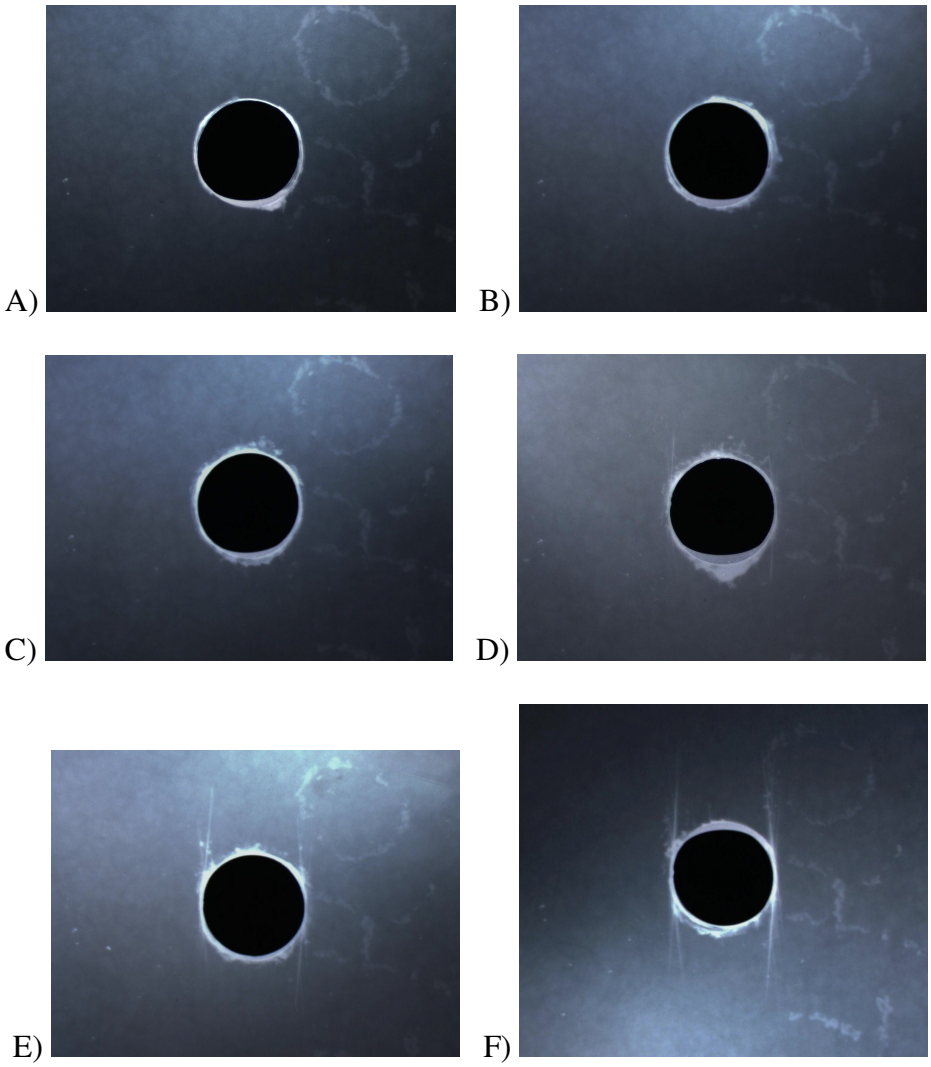

Figure 3.5 Radiographic images around 6.35mm diameter notch for an 80/20 Filled Hole Fully Reversed Damage Initiation Test (SN4). a) 0 kN (new specimen) b) 50k cycles at first stress level c) 50k cycles at second stress level d) 50k cycles at third stress level e) 50k cycles at fourth stress level (crack > 0.5" or 1.27cm) f) 1 million cycles at fourth stress level.

3.4.4 Definition of Longitudinal Split Length

For all of the in-situ radiographic images taken, the split length was measured and recorded. Split length was defined as the longest vertical distance between crack tips due to longitudinal splitting.

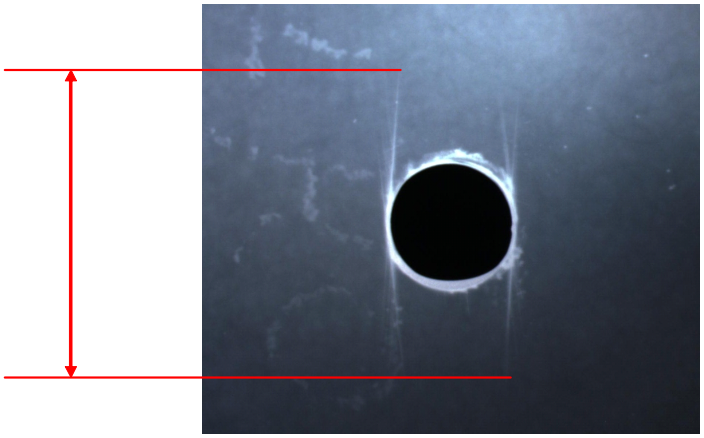

Figure 3.6 Example of the split length measured from a typical x-ray around the notch in a carbon fiber coupon specimen

3.4.5 Justification of Split Length as Damage Parameter

Previous work has been done to show the difference in damaged states between "soft", "medium", and "hard" laminates. The more longitudinal fibers there are in a specimen, the "harder" the laminate. Using an IM-7 carbon fiber system, past researchers showed that longitudinal splitting was the predominant form of damage in "hard" layups [Etheridge]. Table 3.1 shows the laminates, as well as their stacking sequences and number/percent of longitudinal plies.

Table 3.1: Soft/Medium/Hard layups used to highlight different damage states

Laminate	Stacking Sequence	Number of Plies (0/±45/90)	Pct. of Plies (%0/%±45/%90)
Soft	$[(\pm 45)_2/90/-45/0/(\pm 45)_2/45]_S$	(2 / 20 / 2)	(8 / 84 / 8)
Medium	$[45/90/-45/0]_{3S}$	(6 / 12 / 6)	(25 / 50 / 25)
Hard	$[45/0_3/-45/90/45/0_3/-45/0]_S$	(14 / 8 / 2)	(58 / 33 / 8)

As evident in Figure 3.7, as the percentage of longitudinal plies increases, the specimen is more and more likely to crack along those longitudinal plies. The "soft" layup is characterized by transverse cracking, as well as some 45° ply cracking. The "medium layup shows predominantly 45° ply cracks, with smaller longitudinal ones to the left and right of the hole. In the "hard" layup, which is the one most similar to the specimens used for this current project, longitudinal ply cracking determines the extent of damage in the specimen. For this reason, this was chosen as the damage parameter to compare the hard layups 50/40/10, 80/20, and 70/30.

A) 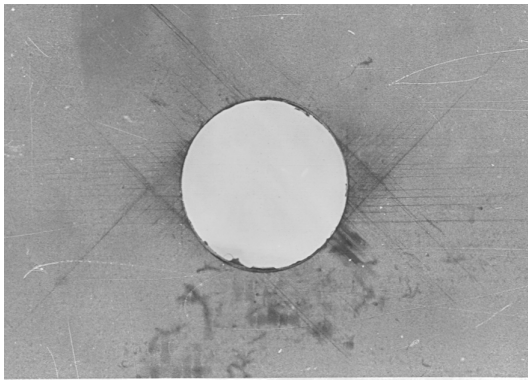 B) 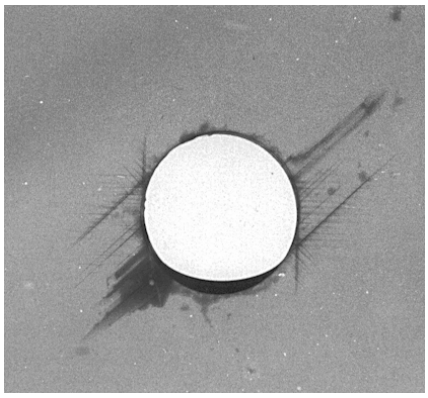

C) 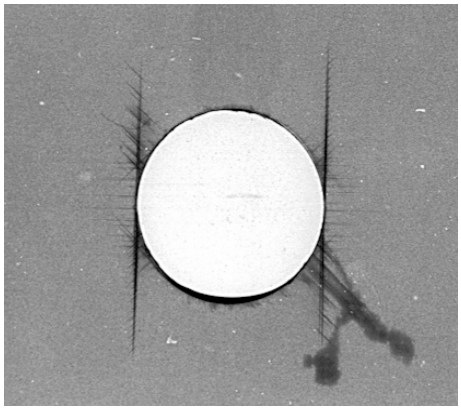

Figure 3.7 Radiographic images around 6.35mm diameter notch for a) “soft” specimen b) “medium” specimen c) “hard” specimen

Chapter 4 : OPEN HOLE RESULTS AND DISCUSSION

This section will cover the results of the open hole tests as well as offer comparisons organized by test conditions.

4.1 Cyclic Open Hole Tension (R = -0.1)

The first set of fatigue tests involved cycling that was mostly performed in tension, with R = -0.1 (a 10% reversal of loading into compression). Figure 4.1 shows the stress at which damage initiates (intersection with x-axis), as well as the stress at which the critical damage criterion is exceeded. The data is normalized to the static ultimate tensile strength of the 50/40/10 composite laminate. For all tests, the dominant mode of damage was splitting on the left and right side of the hole, in the longitudinal direction. This is typical for "hard" composite laminates. Stress concentrations around the notch were the reason damage consistently initiated at these sites. The long-term crack growth, from continued cycling at the highest stress level attained, is designated by the vertical portion of the line segment. In these tests, the traditional 50/40/10 laminate withstood a slightly higher absolute stress than either non-traditional laminate. The 80/20 specimen and 50/40/10 specimen each exhibited a similar amount of long-term crack growth after the damage criterion was met, while the 70/30 specimen showed increased long-term growth. Figure 4.2 shows the different splits occurring in each laminate. With the non-traditional laminates (80/20 and 70/30), the split crack tips in different longitudinal plies (+5° and -5° orientations) diverge as the cracks propagates, providing increased resistance to further damage as the splits extend in the longitudinal direction.

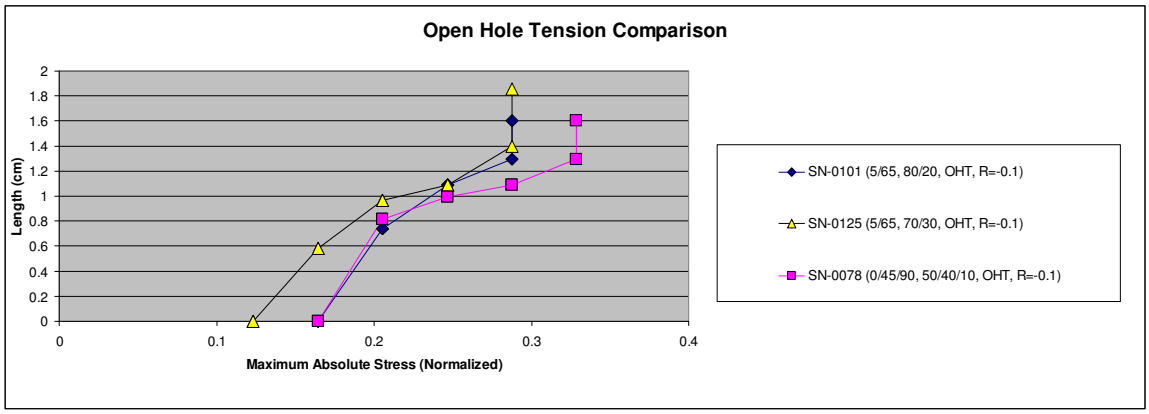

Figure 4.1 Open Hole Tension (OHT) tests (Specimen, Layup, Test type, R ratio)

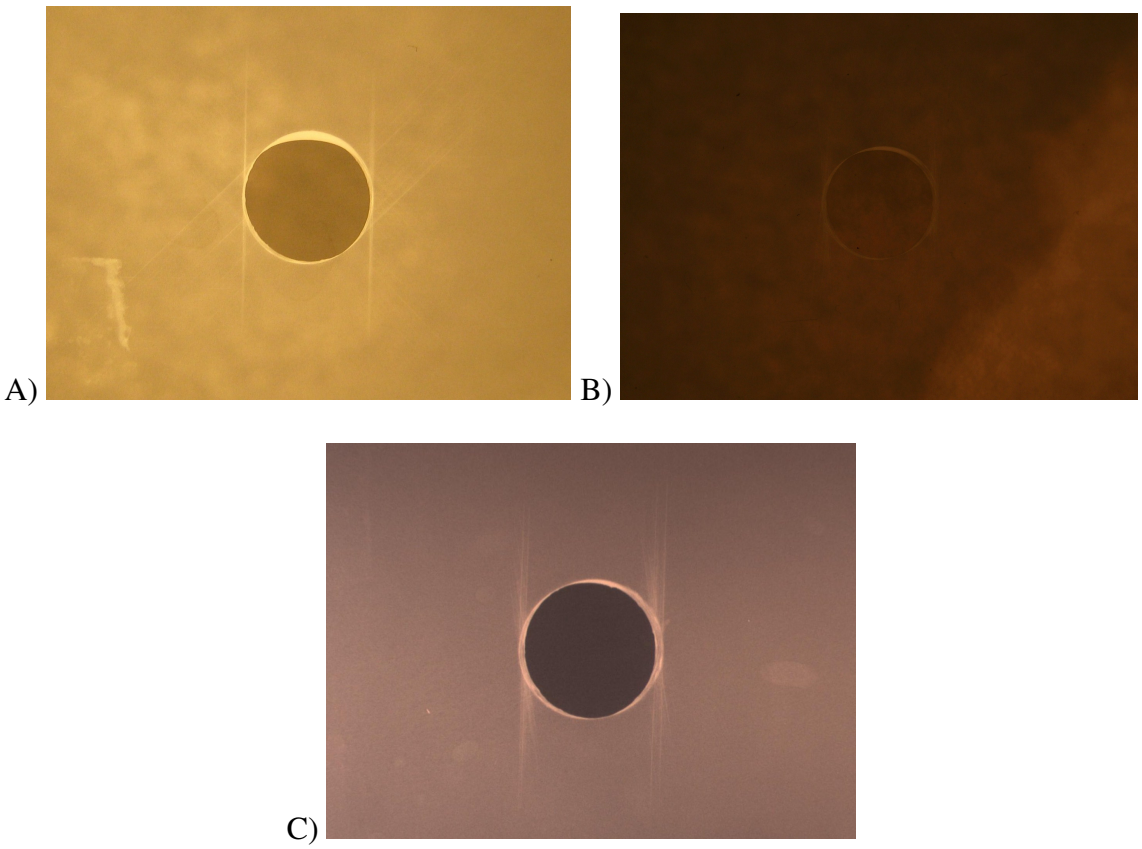

Figure 4.2 Radiographic images around 6.35mm diameter notch after 1 million cycles at max stress in Open Hole Tension for a) 50/40/10 laminate, b) 80/20 laminate, and c) 70/30 laminate.

4.2 Cyclic Open Hole Compression (R = -10)

The second set of testing included fatigue testing the specimen mostly in compression, with R = -10 (10% reversal into tension). Figure 4.3 shows the corresponding split growth data acquired at each stress level. As before, stress levels for damage initiation and those required for surpassing the damage criterion of 1.27 cm (0.5") are clearly evident. The data is normalized to the static ultimate compressive strength of the 50/40/10 composite laminate.

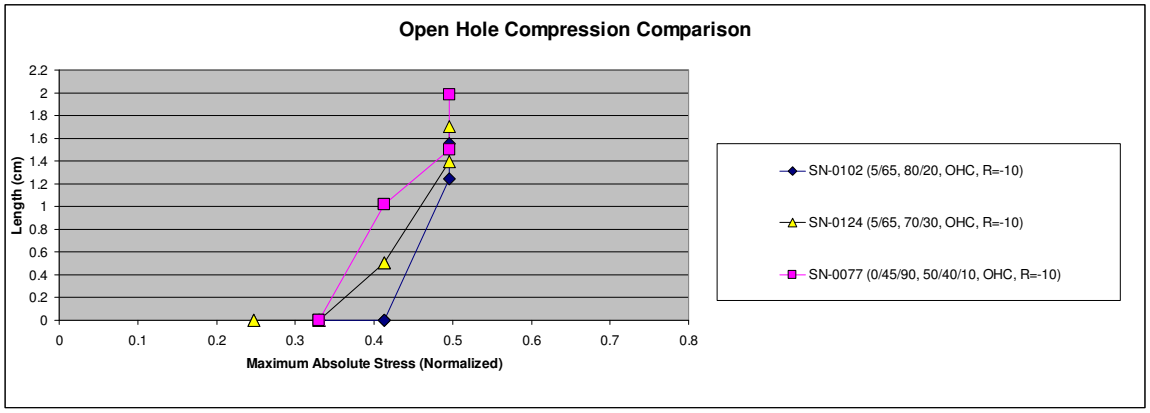

Figure 4.3 Open Hole Compression (OHC) tests (Specimen, Layup, Test type, R ratio)

In compression, the 80/20 and 70/30 non-traditional laminates outperformed the typical 50/40/10 configuration by both exhibiting a shorter crack length at the same stress as well as showing a slower long-term crack growth. Figure 4.4 shows the final damage state of each laminate upon completion of the fatigue testing.

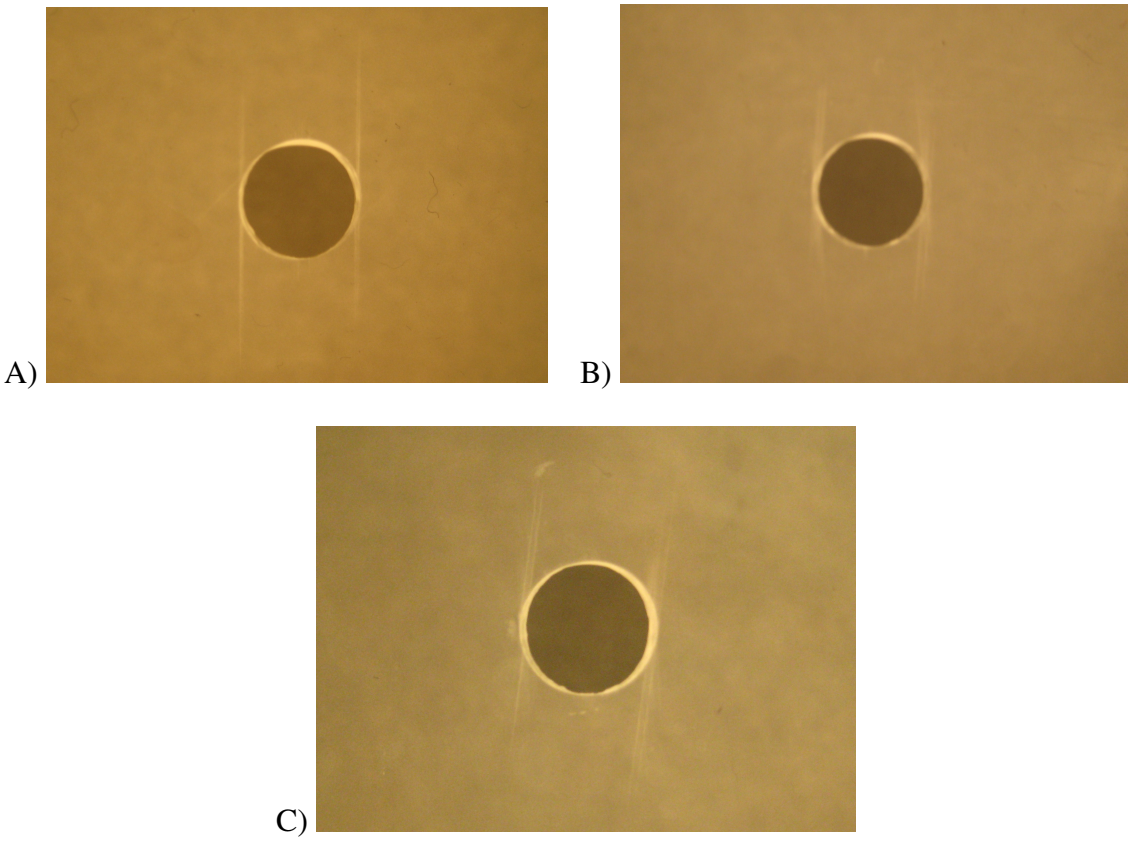

Figure 4.4 Radiographic images around 6.35mm diameter notch after 1 million cycles at max stress in Open Hole Compression for a) 50/40/10 laminate, b) 80/20 laminate, and c) 70/30 laminate.

4.3 Cyclic Open Hole Fully Reversed (R = -1)

Fully Reversed fatigue testing, where R = -1 (equal stresses in tension and compression), separated the traditional and non-traditional laminates. Figure 4.5 compares the length of the longitudinal splitting across the different specimens. The data is normalized to the static ultimate tensile strength of the 50/40/10 composite laminate. The 80/20 and 70/30 laminates behaved almost identically, while the 50/40/10 consistently had less damage at the same stress level and was able to surpass the maximum stress achieved (before reaching the 1.27cm or 0.50" criteria) in the non-traditional laminates.

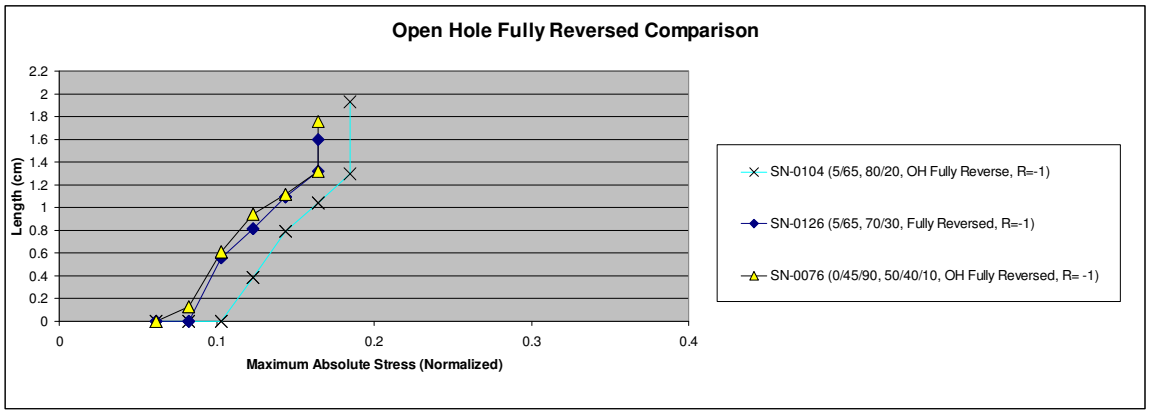

Figure 4.5 Open Hole Fully Reversed tests (Specimen, Layup, Test type, R ratio)

The final damage state of each laminate is shown in Figure 4.6. The 50/40/10 has very defined splits, corresponding to the cracks in individual plies being aligned with one another. The non-traditional ones show divergent crack paths as the splits lengthen.

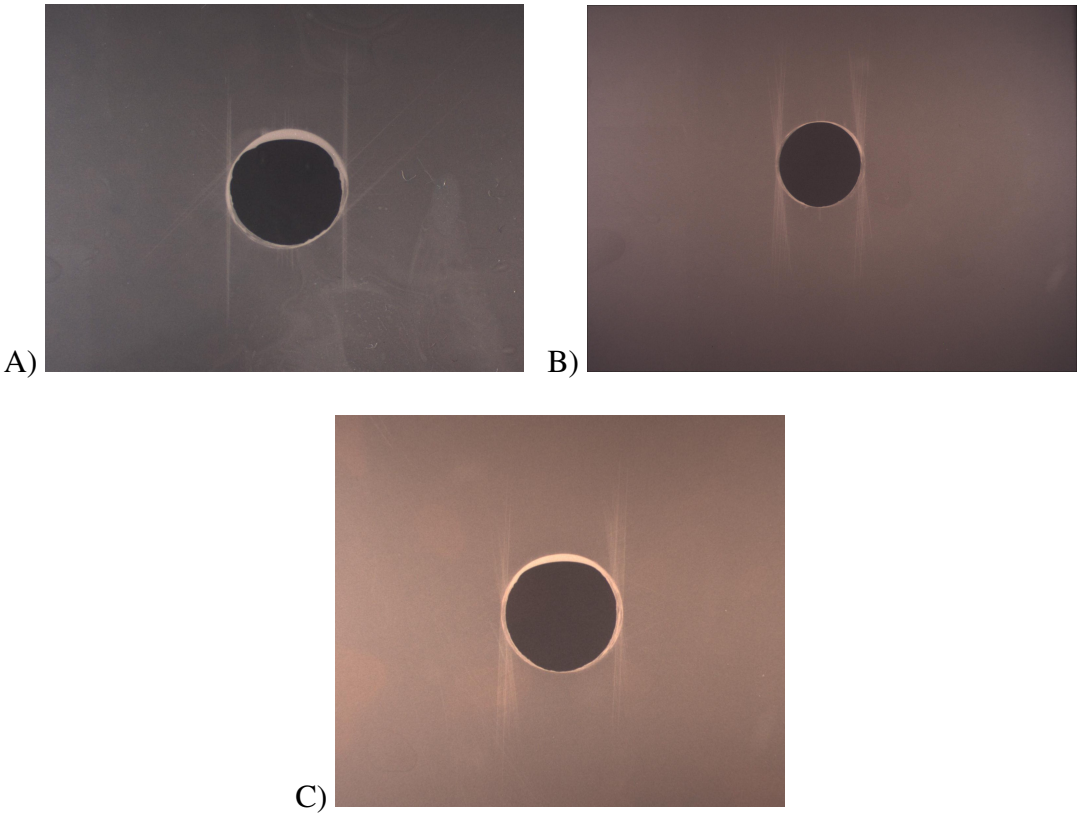

Figure 4.6 Radiographic images around 6.35mm diameter notch after 1 million cycles at max stress Open Hole Fully Reversed for a) 50/40/10 laminate, b) 80/20 laminate, and c) 70/30 laminate.

4.4 Cyclic Open Hole Mostly Tension (R = -0.35)

Each layup was also tested at R= -0.35, which is predominantly tension (approximately three-fourths of the stress range is in tension). For this stress ratio, the non-traditional 80/20 laminate outperformed the traditional 50/40/10 at crack initiation by showing no damage until a higher stress level was reached. Both specimens had similar splitting damage at higher stresses, at which they reached the critical damage criteria and summarily cycled for 1 million total cycles at that stress level. Figure 4.7 shows the damage plots. The data is normalized to the static ultimate tensile strength of the 50/40/10 composite laminate.

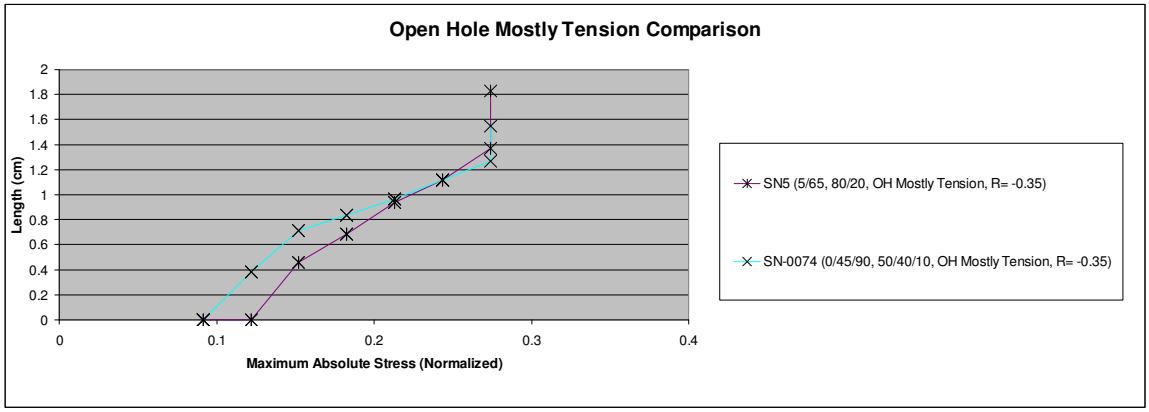

Figure 4.7 Open Hole Mostly Tension tests (Specimen, Layup, Test type, R ratio)

Shown in Figure 4.8 are the in-situ x-rays of the notched composite specimens after completing the low-cycle stress variations as well as the long-term fatigue testing at the maximum stress reached. In regard to the obvious difference in images, this was also the first time a comparison was drawn between an x-ray taken with the older Polaroid film and the newer Kodak film.

This test also was the first to not include the 70/30 laminate. After comparing the three laminates at R = -0.1 and R = -10 and R = -1, the two non-traditional ones were very similar in behavior across different stress ranges. Due to the higher stiffness of the 80/20, it was decided that the test matrix would narrow to only the 80/20 and the traditional 50/40/10 laminate across a longer list of stress ratios.

A) 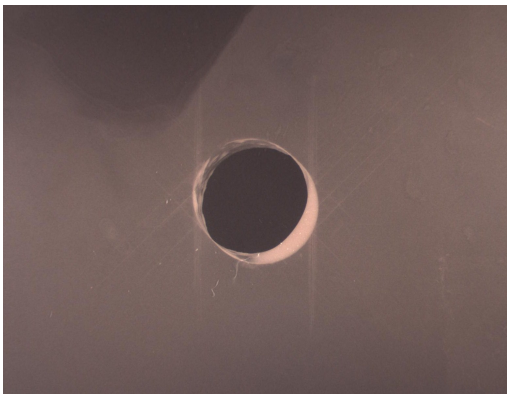 B) 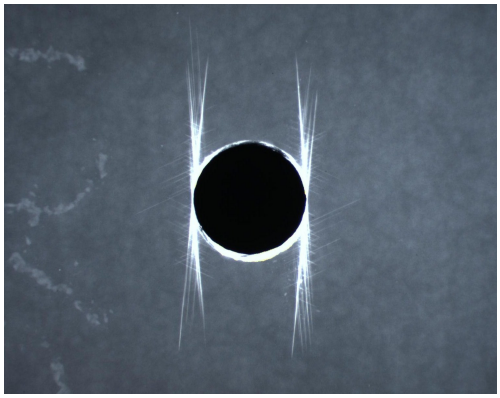

Figure 4.8 Radiographic images around 6.35mm diameter notch after 1 million cycles at max stress Mostly Tension Fully Reversed for a) 50/40/10 laminate, b) 80/20 laminate.

4.5 Cyclic Open Hole Mostly Compression (R = -3)

Another interesting stress ratio is R = -3, which means three-fourths of the stress range is in compression. During this set of testing (plotted in Figure 4.9), the traditional 50/40/10 laminate withstood an extra increment of cycling before damage initiated, as well as reaching a higher stress level before surpassing the damage criteria of 1.27cm (0.50") total split length. The data is normalized to the static ultimate compressive strength of the 50/40/10 composite laminate.

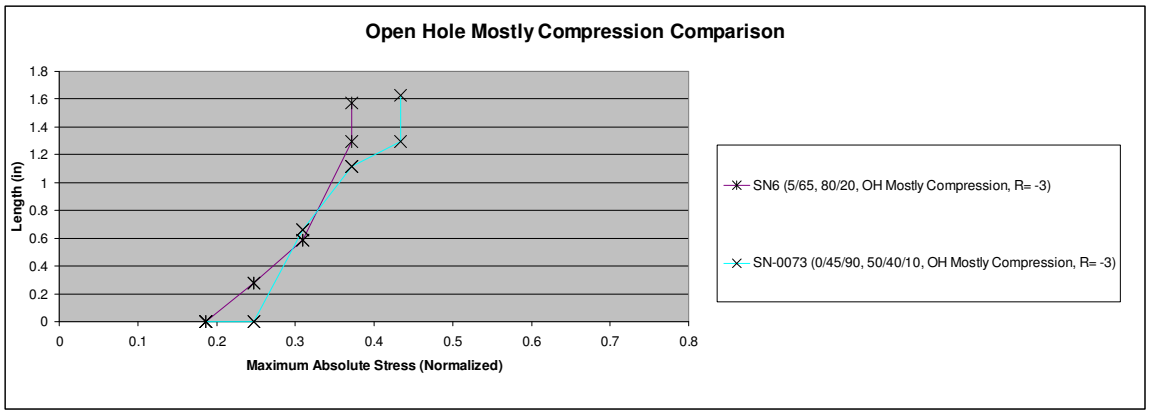

Figure 4.9 Open Hole Mostly Compression tests (Specimen, Layup, Test type, R ratio)

The x-rays in Figure 4.10 show a very similar damage state, with the only difference being off-axis path of the splits in the non-traditional laminate. One important distinction is that the 50/40/10 traditional one cycled one stress increment higher and yet is no more damaged than its counterpart.

A) 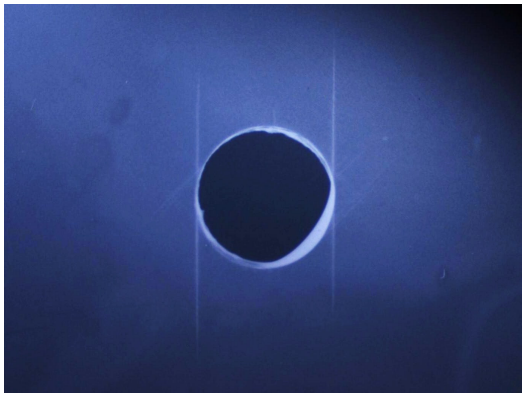 B) 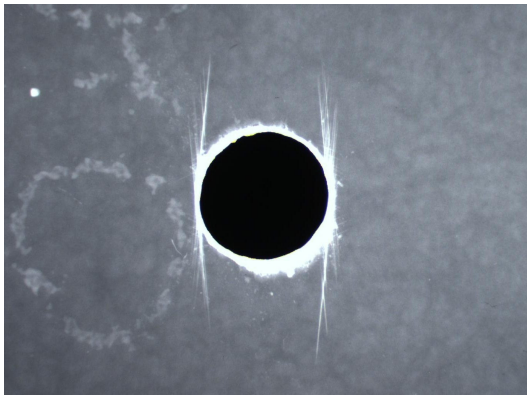

Figure 4.10 Radiographic images around 6.35mm diameter notch after 1 million cycles at max stress Open Hole Mostly Compression for a) 50/40/10 laminate, b) 80/20 laminate

Chapter 5 : FILLED HOLE RESULTS AND DISCUSSION

This section will discuss the performance of the different laminates under filled hole conditions and show comparison data.

5.1 Cyclic Filled Hole Tension (R = -0.1)

While open hole results provided a baseline for damage propagation in composite laminates, filled hole tests provided more realistic data that is closer to structural applications across the aerospace, automotive, and naval industry. Filled hole testing enabled the researchers to make numerous more comparisons across and within the laminates in the test matrix. As in open hole testing, the predominant damage mode was longitudinal splitting with the splits originating on the sides of the hole. For filled hole tension (R = -0.1), the traditional 50/40/10 laminate significantly outperformed the 80/20 laminate. While both specimens initiated damage at the same stress level, the traditional specimen reached 25% higher stress before it crossed the 1.27cm (0.50") split length. Both specimens exhibited slower long-term crack growth than their open hole counterparts. The filled hole plots are shown in Figure 5.1. The data is normalized to the static ultimate tensile strength of the 50/40/10 composite laminate.

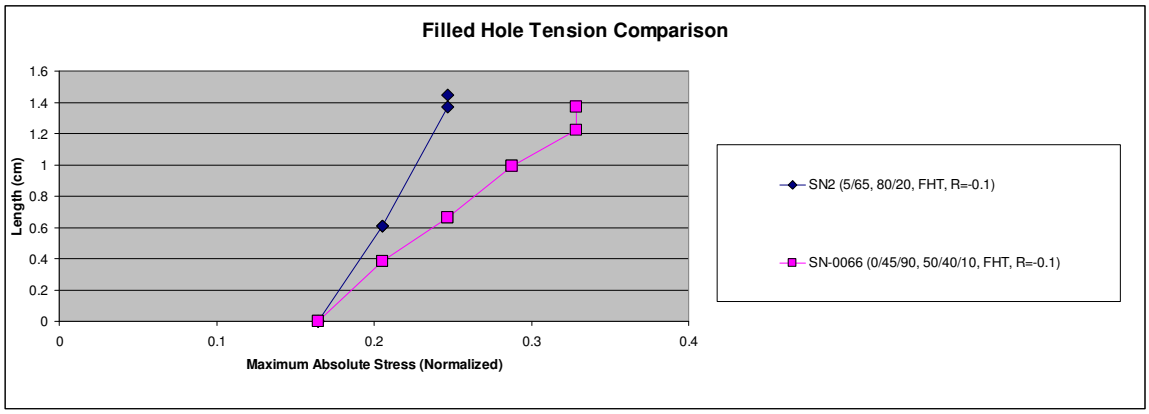

Figure 5.1 Filled Hole Tension tests (Specimen, Layup, Test type, R ratio)

After 1 million cycles at the maximum stress reached before exceeding the damage criteria, both laminates showed minimal long-term crack growth. The damaged zone around the central notch can be seen in Figure 5.2. The "damage" right around the hole is surface wear from the fastener. The real damage is the longitudinal splitting on the sides and the top and bottom of the hole.

A) 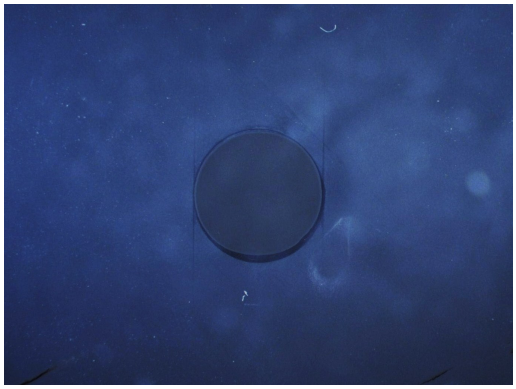 B) 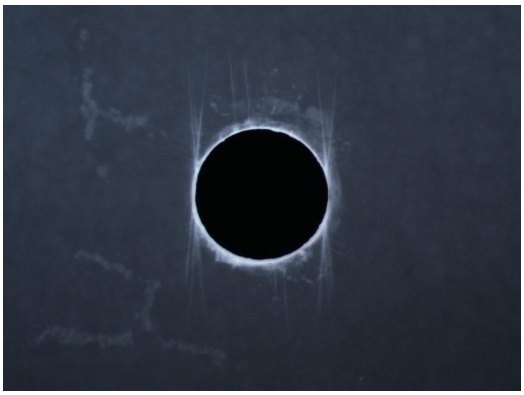

Figure 5.2 Radiographic images around 6.35mm diameter notch after 1 million cycles at max stress Tension for a) 50/40/10 laminate, b) 80/20 laminate

5.2 Cyclic Filled Hole Compression (R = -10)

Filled Hole Compression provided another comparison of traditional vs. non-traditional composite laminate fatigue performance. As visible in Figure 5.3, the 80/20 laminate showed a much higher damage initiation stress as well as a higher maximum stress allowable before the long-term crack growth portion of the test procedure. The 50/40/10 showed a fairly linear progression of damage. The 80/20, once it damaged, showed a drastic jump in longitudinal splitting. The data is normalized to the static ultimate compressive strength of the 50/40/10 composite laminate.

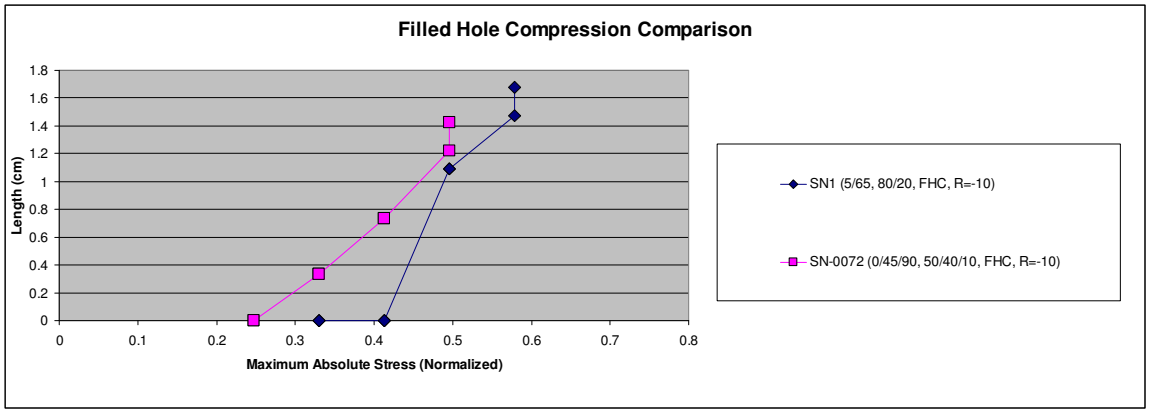

Figure 5.3 Filled Hole Compression tests (Specimen, Layup, Test type, R ratio)

The final x-rays of each specimen, shown in Figure 5.4, displayed damage patterns that were similar to the open hole testing. The filled hole tests also showed surface wear from the fastener. While the 80/20 laminate had a longer split length, it did cycle at a higher stress level.

A) 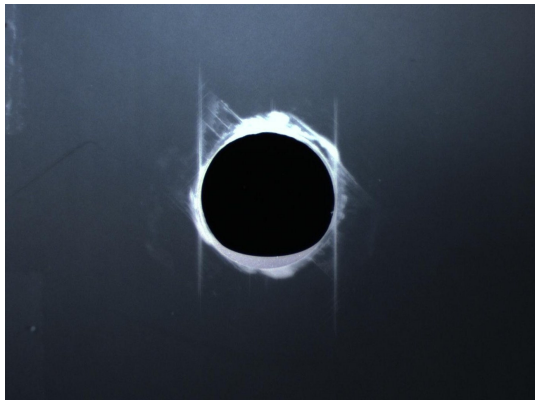 B) 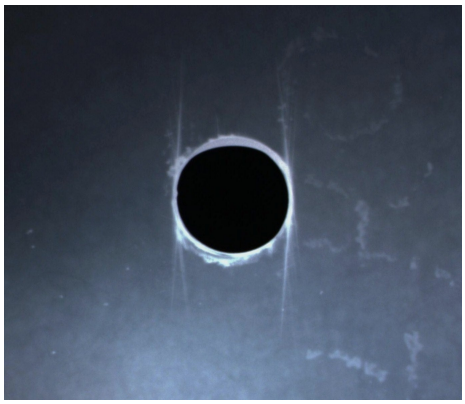

Figure 5.4 Radiographic images around 6.35mm diameter notch after 1 million cycles at max stress Compression for a) 50/40/10 laminate, b) 80/20 laminate

5.3 Cyclic Filled Hole Fully Reversed (R = -1)

Fully Reversed testing (equal percentage of stress range in tension as in compression) was also performed with filled hole specimens. In this case, the 50/40/10 laminate survived two additional stress levels, compared to the 80/20, before reaching the damage criteria. The 50/40/10 showed a linear and predictable crack growth with increasing stress. Both showed less long-term crack growth compared to their open hole counterparts. The plots are shown in the Figure 5.5. The data is normalized to the static ultimate tensile strength of the 50/40/10 composite laminate.

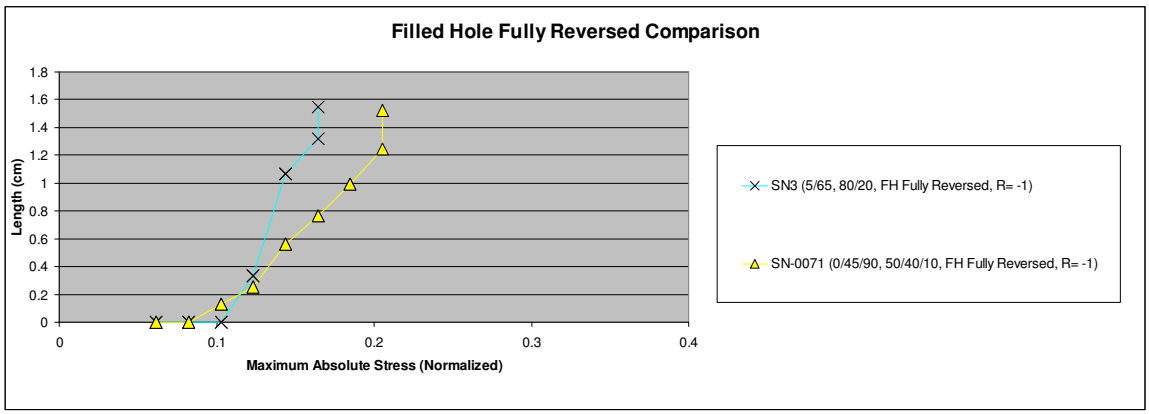

Figure 5.5 Filled Hole Fully Reversed tests (Specimen, Layup, Test type, R ratio)

Final x-rays of the two specimens showed ordinary splitting around the hole, with some surface wear from the fastener. Cracks in 45° plies (for the 50/40/10) as well as splitting from the bottom of the 80/20 hole are visible, as shown in Figure 5.6.

A) 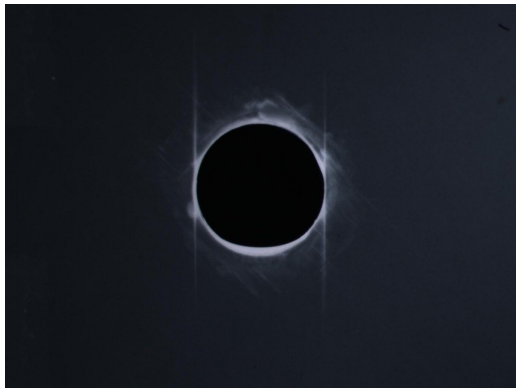 B) 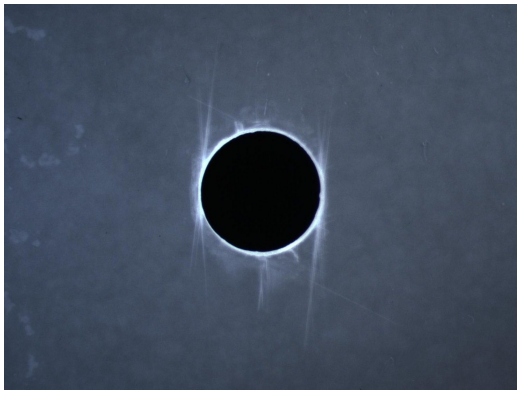

Figure 5.6 Radiographic images around 6.35mm diameter notch after 1 million cycles at max stress Fully Reversed for a) 50/40/10 laminate, b) 80/20 laminate

5.4 Cyclic Filled Hole Mostly Tension (R = -0.35)

For the Filled Hole Mostly Tension tests (R = -0.35), both specimens initiated damage at the same stress level, which was equal to or better than their open hole equivalents. While they displayed very similar damage lengths, the 80/20 did accumulate more damage than the 50/40/10 specimen at higher stresses and also had a larger long-term crack growth during the final stage of testing at the highest stress for 1 million cycles. These trends are plotted in Figure 5.7. The data is normalized to the static ultimate tensile strength of the 50/40/10 composite laminate.

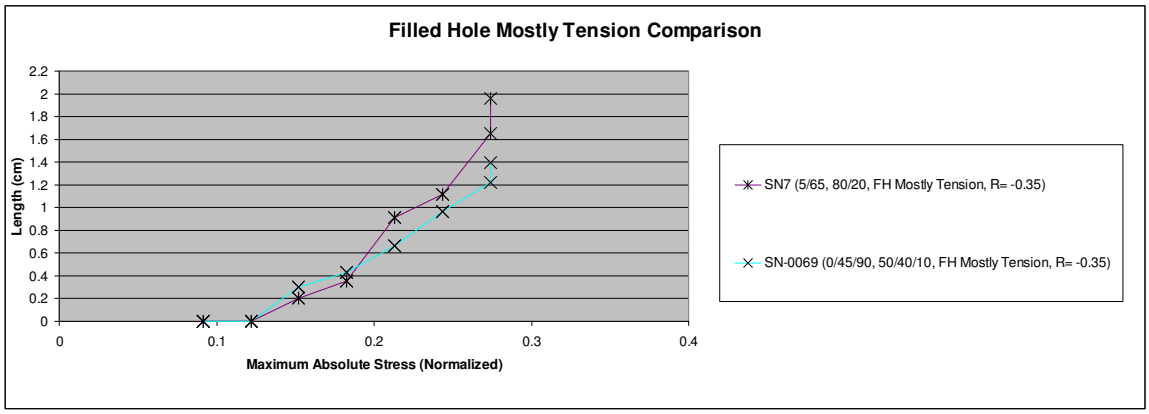

Figure 5.7 Filled Hole Mostly Tension tests (Specimen, Layup, Test type, R ratio)

Figure 5.8 shows the difference between the two laminates after completing the Damage Initiation Method of incremental stress followed by long-term fatigue. Extensive cracking in the 45° plies is visible for the traditional specimen.

A) 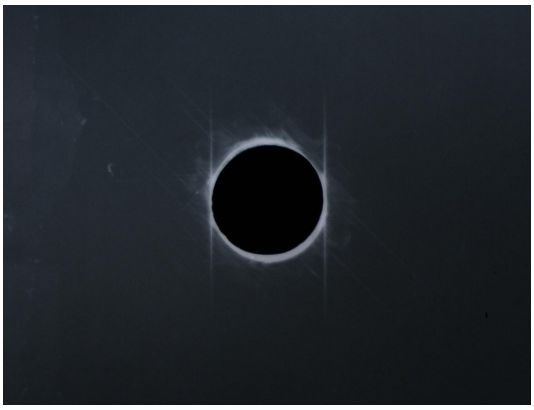 B) 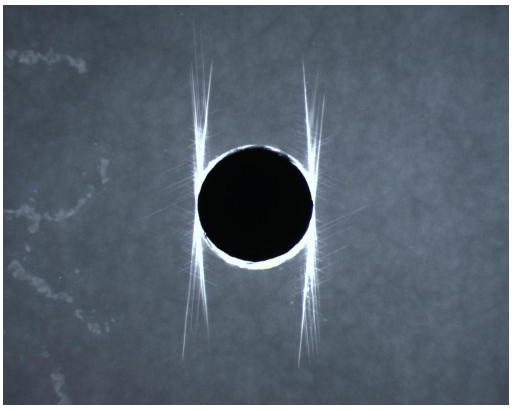

Figure 5.8 Radiographic images around 6.35mm diameter notch after 1 million cycles at max stress Mostly Tension for a) 50/40/10 laminate, b) 80/20 laminate

5.5 Cyclic Filled Hole Mostly Compression (R = -3)

The Filled Hole Mostly Compression tests (R = -3) maintained the same gap in performance between the traditional and non-traditional laminates that were seen in the open hole testing. However, both specimens increased their maximum stress and showed

slightly more linear damage progression with regard to increasing stress levels. This was documented in Figure 5.9. The data is normalized to the static ultimate compressive strength of the 50/40/10 composite laminate.

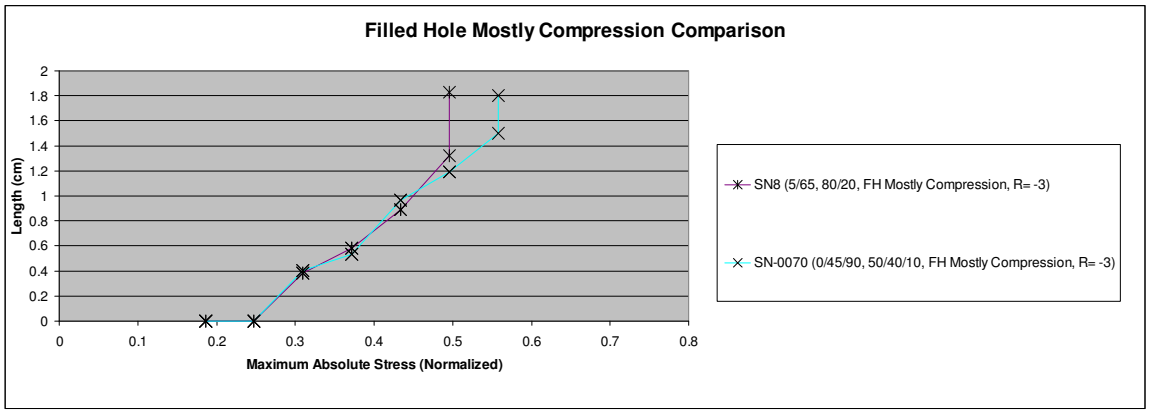

Figure 5.9 Filled Hole Mostly Compression tests (Specimen, Layup, Test type, R ratio)

Final x-rays captured the damage that accumulated throughout the testing. These are shown in Figure 5.10. One interesting note was that the non-traditional 80/20 specimen showed cracking in the 65° plies (to the lower right of the picture). This was the only test in which the stress applied was able to sufficiently fatigue the 65° plies and cause cracking.

A) 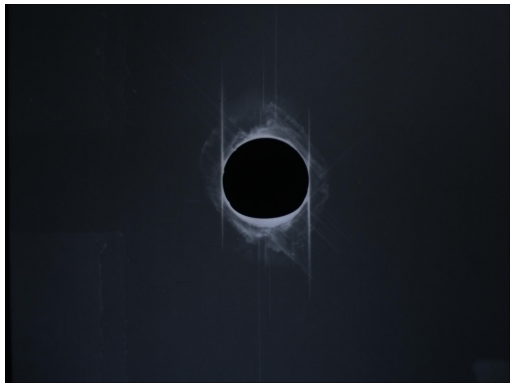 B) 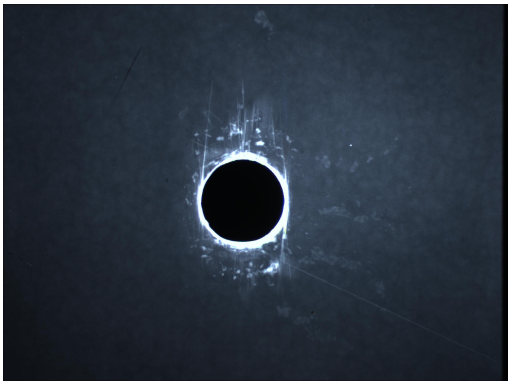

Figure 5.10 Radiographic images around 6.35mm diameter notch after 1 million cycles at max stress Mostly Compression for a) 50/40/10 laminate, b) 80/20 laminate

Chapter 6 : FILLED VERSUS OPEN HOLE COMPARISONS

This section will discuss the performance of the different laminates under filled hole and open hole conditions and show comparison data between the two conditions.

6.1 Open versus Filled Hole Tension

6.1.1 50/40/10 Laminate (R = -0.1)

Comparing the 50/40/10 laminate in Open versus Filled Hole Tension, the Filled Hole specimen consistently has a shorter crack length at the same stress level. Also, the long-term crack growth was not as severe. Both observations were seen in Figure 6.1. The data is normalized to the static ultimate tensile strength of the 50/40/10 composite laminate.

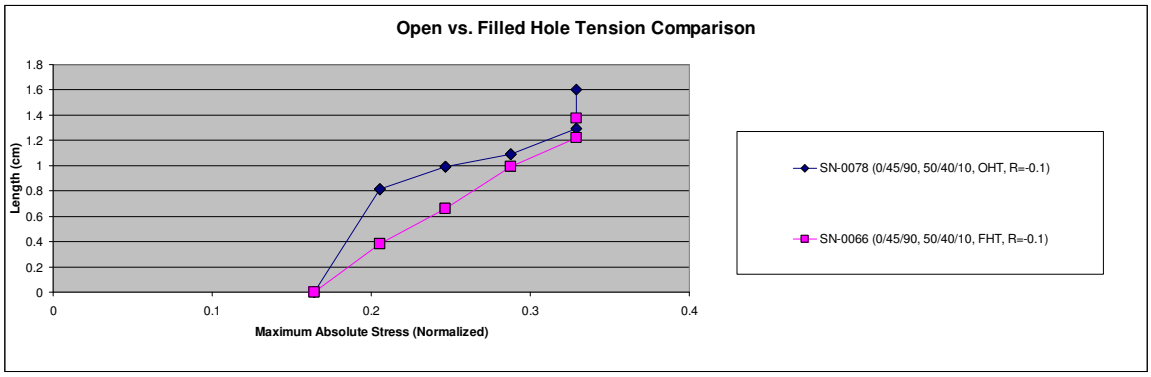

Figure 6.1 Open versus Filled Hole Tension tests (Specimen, Layup, Test type, R ratio)

The two x-rays of the final damage states of the specimens, shown in Figure 6.2, showed the same modes of damage, with the open hole specimen displaying a longer crack length. Also, cracking in the off-axis plies was more severe for the filled hole specimen.

This could be due to the fastener changing the stress state around the hole and causing higher shear stresses in the 45° plies.

A) 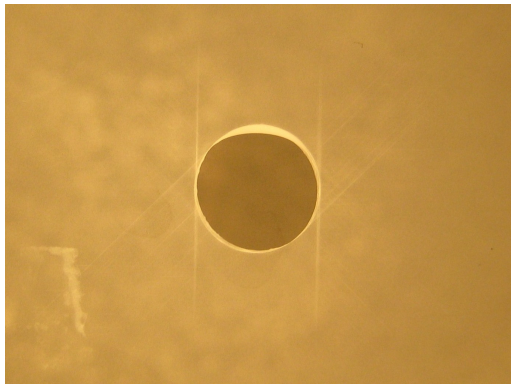 B) 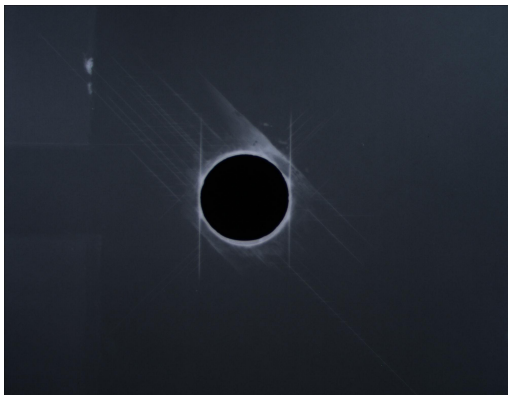

Figure 6.2 Radiographic images around 6.35mm diameter notch after 1 million cycles at max stress Tension for a) Open Hole specimen, b) Filled Hole specimen

6.1.2 80/20 Laminate (R = -0.1)

Comparing the 80/20 laminate in Open versus Filled Hole Tension, the Filled Hole specimen actually reached the damage criteria sooner than the open hole version. However, the filled hole specimen had significantly less crack growth while long-term cycling. Both observations were seen in the chart in Figure 6.3. The data is normalized to the static ultimate tensile strength of the 80/20 composite laminate.

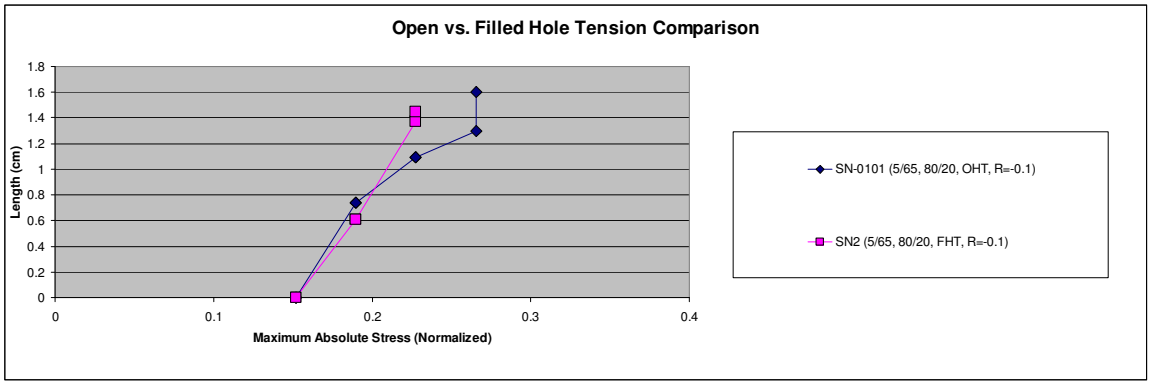

Figure 6.3 Open versus Filled Hole Tension tests (Specimen, Layup, Test type, R ratio)

The x-rays shown in Figure 6.4 highlight the difference between the open and filled hole tests. In the filled hole test, cracks originate from the top and bottom of the hole, while these were not present in the open hole. With a fastener installed, the stress would flow not only around the hole, but also across the fastener, and possibly crack the plies at the top and bottom of the hole.

A) 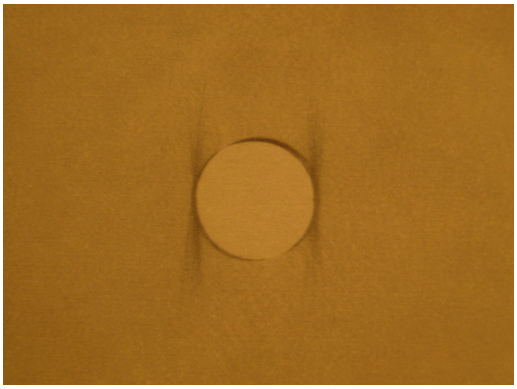 B) 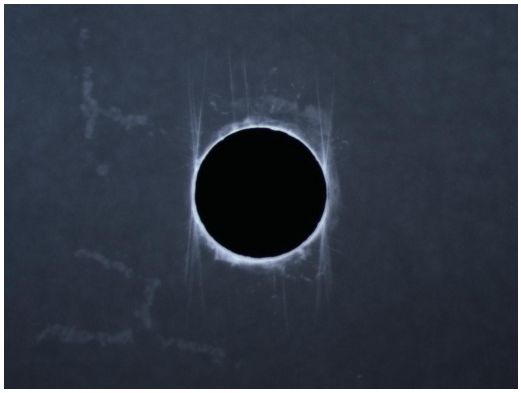

Figure 6.4 Radiographic images around 6.35mm diameter notch after 1 million cycles at max stress Tension for a) Open Hole specimen, b) Filled Hole specimen

6.2 Open versus Filled Hole Compression

6.2.1 50/40/10 Laminate (R = -10)

Comparing the 50/40/10 laminate in Open versus Filled Hole Compression, the Filled Hole specimen initiated damage first. It also had a slower crack growth rate as stress increased, thus allowing it to achieve a shorter crack length at maximum stress. Again, the long-term crack growth in the filled hole test was less than the open hole one. The crack plots are shown in Figure 6.5. The data is normalized to the static ultimate compressive strength of the 50/40/10 composite laminate.

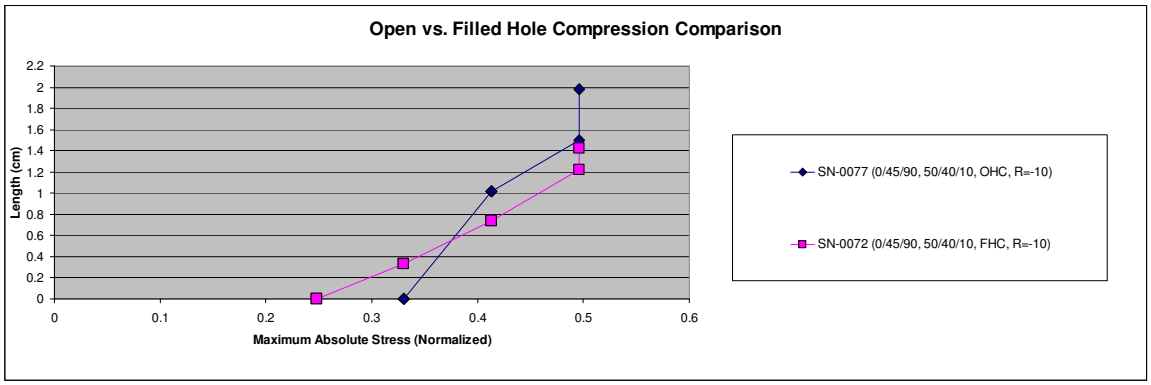

Figure 6.5 Open versus Filled Hole Compression tests (Specimen, Layup, Test type, R ratio)

The two x-rays of the final damage states are shown in Figure 6.6. Similar damage states exist for both, but the filled hole test has more cracking in the off-axis plies. As before, this could be due to the fastener carrying some of the longitudinal loading and transferring stress to the top and bottom of the hole. These are the crack initiation locations of the 45° shears.

A) 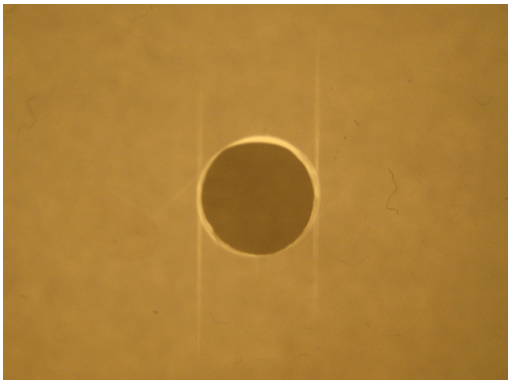 B) 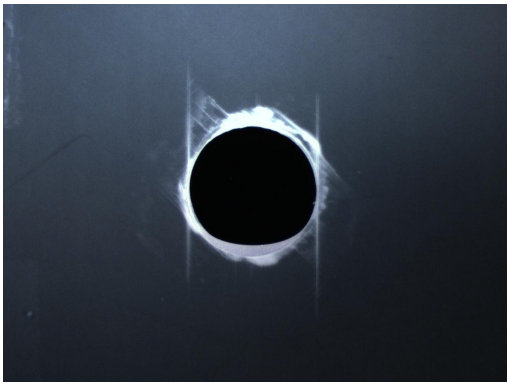

Figure 6.6 Radiographic images around 6.35mm diameter notch after 1 million cycles at max stress Compression for a) Open Hole specimen, b) Filled Hole specimen

6.2.2 80/20 Laminate (R = -10)

Comparing the 80/20 laminate in Open versus Filled Hole Compression, both specimens initiated damage at the same stress level. The filled hole test had a slightly lower crack growth, and thus achieved one more stress increment. The long-term crack growth of the filled hole test was slightly less than the open hole one. See Figure 6.7 for the plotted data. The data is normalized to the static ultimate compressive strength of the 80/20 composite laminate.

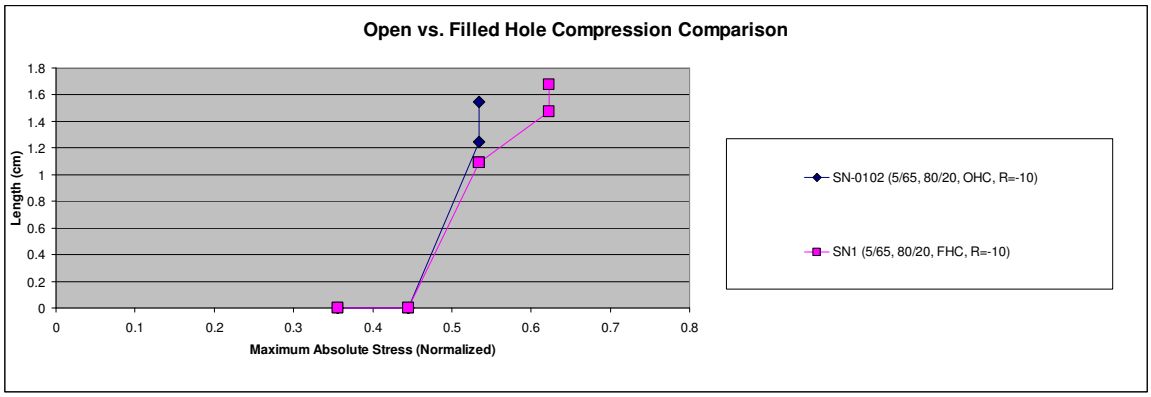

Figure 6.7 Open versus Filled Hole Compression tests (Specimen, Layup, Test type, R ratio)

The two x-rays of the final damage states can be seen in Figure 6.8. Longitudinal cracking was similar for both, and neither test showed cracking in 65° plies or cracks at the top/bottom of the hole.

A) 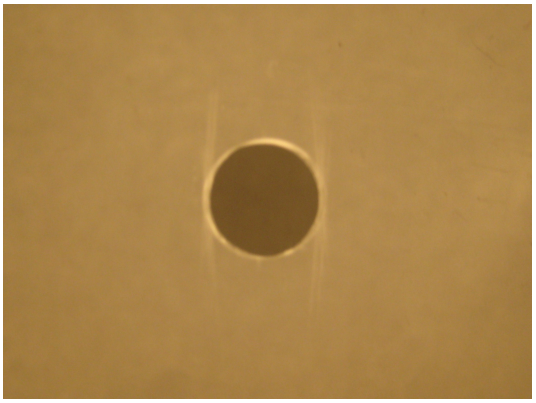 B) 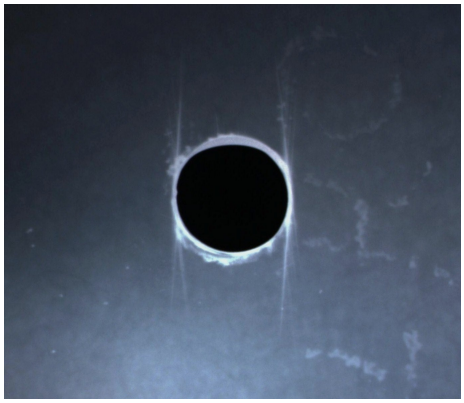

Figure 6.8 Radiographic images around 6.35mm diameter notch after 1 million cycles at max stress Compression for a) Open Hole specimen, b) Filled Hole specimen

6.3 Open versus Filled Hole Fully Reversed

6.3.1 50/40/10 Laminate (R = -1)

Comparing the 50/40/10 laminate in Open versus Filled Hole Fully Reversed Stress, both specimens initiated damage at the same stress level. The filled hole specimen, again, displayed a slower crack growth rate for both the incremental stress tests as well as the long-term fatigue testing. The crack plots are shown in Figure 6.9. The data is normalized to the static ultimate tensile strength of the 50/40/10 composite laminate.

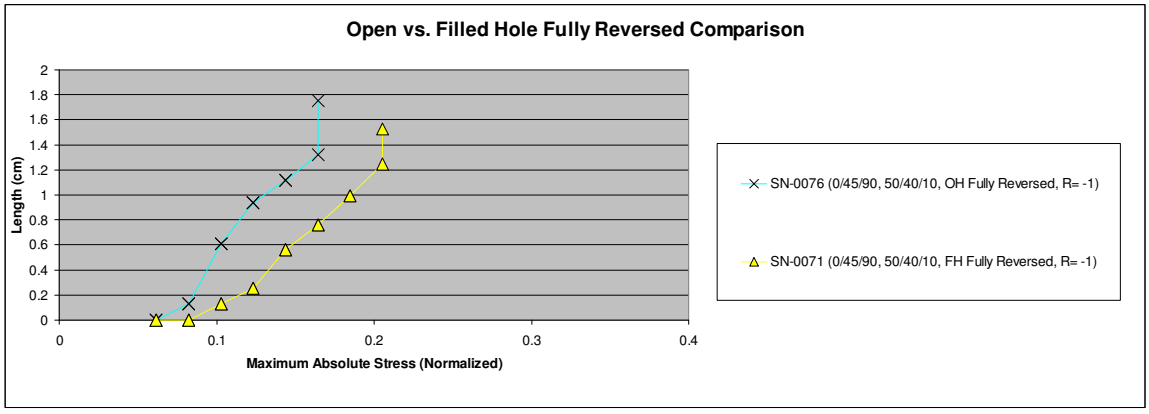

Figure 6.9 Open versus Filled Hole Fully Reversed tests (Specimen, Layup, Test type, R ratio)

In-situ x-rays of the completed tests are shown in Figure 6.10. There are no significant differences between the two. Both have longitudinal splitting and cracks in off-axis plies. The filled hole specimen does have surface wear around the hole, which is typical for all filled hole tests.

A) 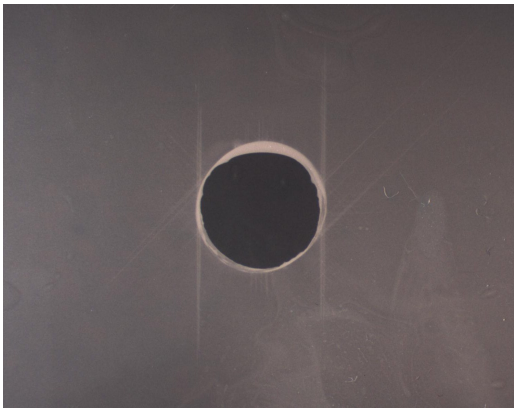 B) 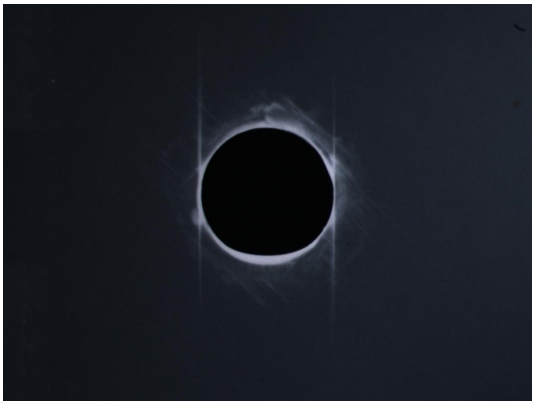

Figure 6.10 Radiographic images around 6.35mm diameter notch after 1 million cycles at max stress Fully Reversed for a) Open Hole specimen, b) Filled Hole specimen

6.3.2 80/20 Laminate (R = -1)

Comparing the 80/20 laminate in Open versus Filled Hole Fully Reversed Stress, damage initiation occurred at the same stress level. The splitting in the filled hole test was more severe, which was not consistent with trends seen at the other stress ratios. The long-term crack growth of the filled hole test was less than half of the open hole crack growth during the long-term fatigue. Figure 6.11 shows the trends seen for this comparison. The data is normalized to the static ultimate tensile strength of the 80/20 composite laminate.

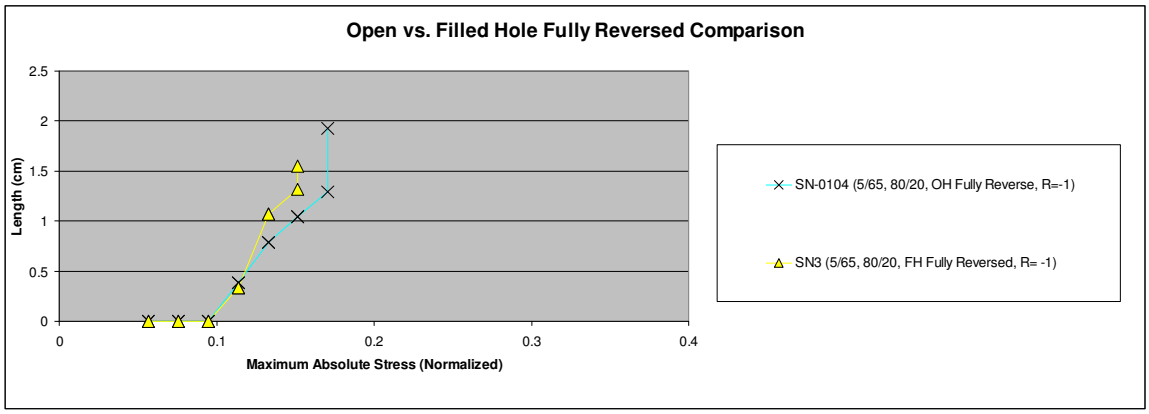

Figure 6.11 Open versus Filled Hole Fully Reversed tests (Specimen, Layup, Test type, R ratio)

X-rays of the two specimens can be compared in Figure 6.12. The filled hole specimen has a shorter crack length, partly due to a lower stress level as well as the fastener carrying stress away from the longitudinal fibers left and right of the hole. The filled hole test showed cracks initiating at the top and bottom of the hole, indicating stress transfer across the fastener and/or localized compression at the top and bottom of the hole due to Poisson effects.

A) 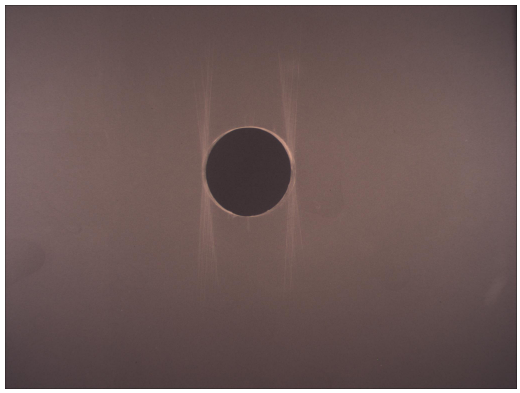 B) 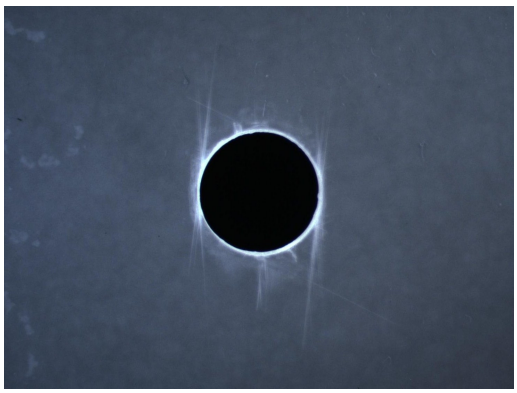

Figure 6.12 Radiographic images around 6.35mm diameter notch after 1 million cycles at max stress Fully Reversed for a) Open Hole specimen, b) Filled Hole specimen

6.4 Open versus Filled Hole Mostly Tension

6.4.1 50/40/10 Laminate (R = -0.35)

Comparing the 50/40/10 laminate in Open versus Filled Hole Mostly Tension Stress, the filled hole specimen initiated damage later than the open hole test. The filled hole test consistently had a shorter crack length across stress levels, and it had a markedly lower long-term growth rate as evidenced in Figure 6.13. The data is normalized to the static ultimate tensile strength of the 50/40/10 composite laminate.

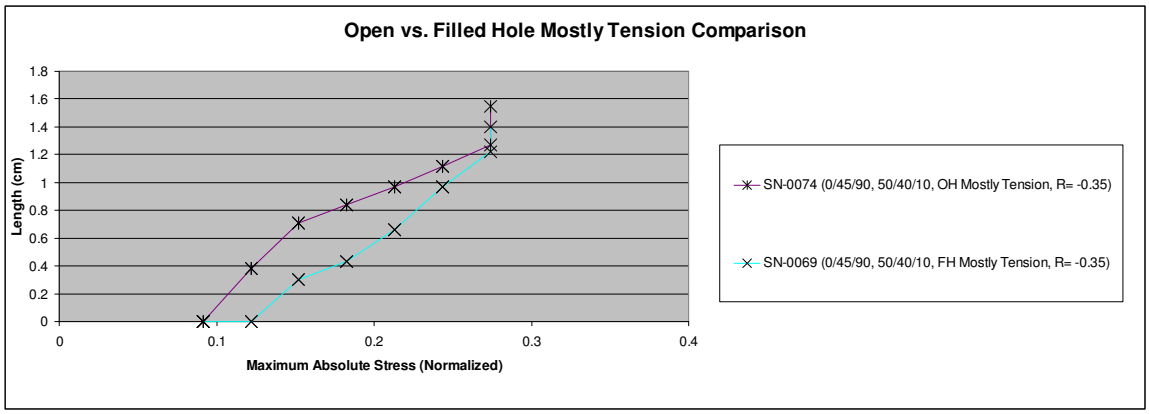

Figure 6.13 Open versus Filled Hole Mostly Tension tests (Specimen, Layup, Test type, R ratio)

X-rays of the two specimens are shown in Figure 6.14. Fatigued at the same maximum stress, the filled hole specimen has a shorter crack length. The fastener carried a portion of the stress across the hole, alleviating some of the stress driving longitudinal crack growth left and right of the notch. Both specimens showed similar cracking in the 45° plies.

A) 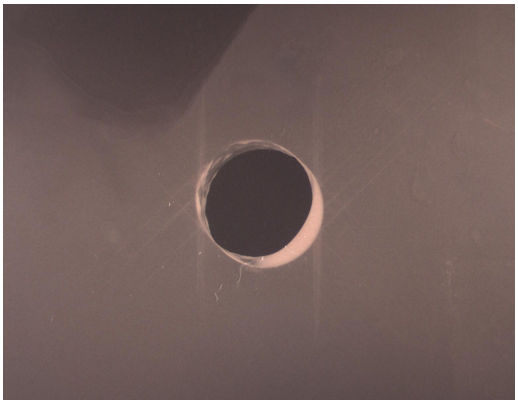 B) 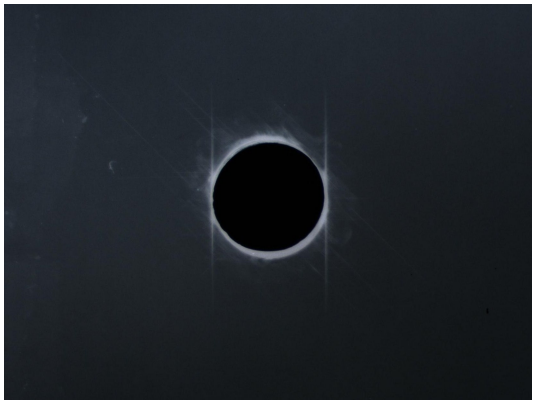

Figure 6.14 Radiographic images around 6.35mm diameter notch after 1 million cycles at max stress Mostly Tension for a) Open Hole specimen, b) Filled Hole specimen

6.4.2 80/20 Laminate (R = -0.35)

Comparing the 80/20 laminate in Open versus Filled Hole Mostly Tension Stress, the two tests initiated damage at the same stress level and closely followed one another to the same stress at which the damage criteria was fulfilled. This data is displayed in Figure 6.15. The filled hole specimen actually had a longer crack length at the maximum stress and at the end of the long-term fatigue testing. The data is normalized to the static ultimate tensile strength of the 80/20 composite laminate.

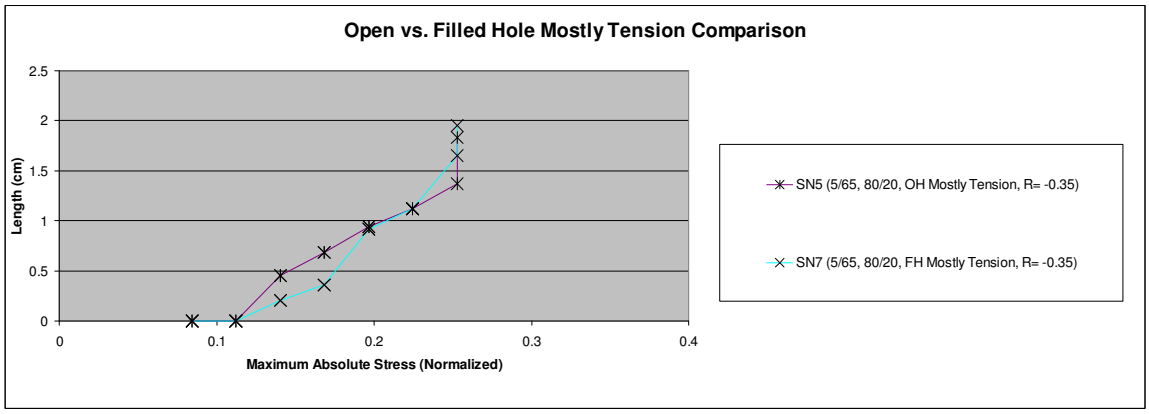

Figure 6.15 Open versus Filled Hole Mostly Tension tests (Specimen, Layup, Test type, R ratio)

Looking at the x-rays, shown in Figure 6.16, the cracks in the open hole test are more pronounced, but the filled hole test has thinner cracks extending further. There was cracking at the top and bottom of the notch in the filled hole specimen, for the same reasons as at other stress ratios: stress transfer across the hole and Poisson effects.

A) 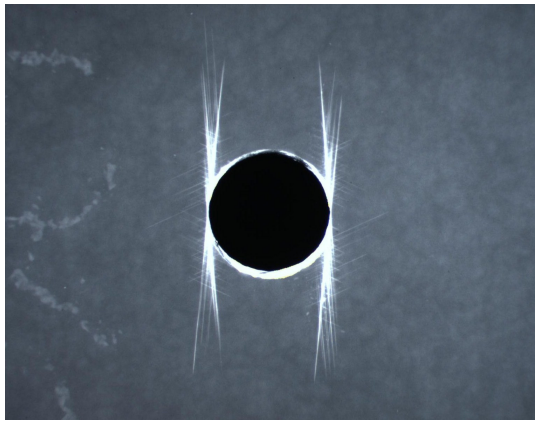 B) 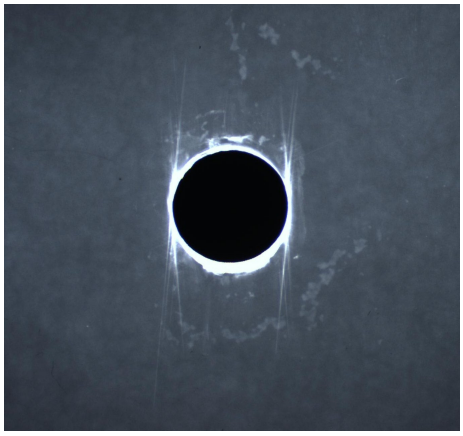

Figure 6.16 Radiographic images around 6.35mm diameter notch after 1 million cycles at max stress Mostly Tension for a) Open Hole specimen, b) Filled Hole specimen

6.5 Open versus Filled Hole Mostly Compression

6.5.1 50/40/10 Laminate (R = -3)

Comparing the 50/40/10 laminate in Open versus Filled Hole Mostly Compression Stress, both tests initiated damage at the same stress level. After that point, the splits in the filled hole test grew at a slower rate with increasing stress increments than its open hole comparison; however, the lower long-term growth rate was almost equal. See Figure 6.17 for more details. The data is normalized to the static ultimate compressive strength of the 50/40/10 composite laminate.

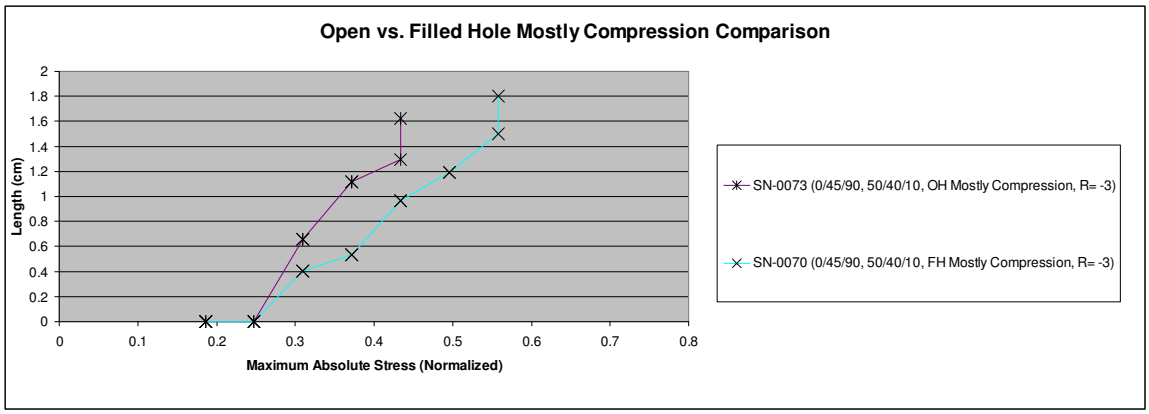

Figure 6.17 Open versus Filled Hole Mostly Compression tests (Specimen, Layup, Test type, R ratio)

As seen in the x-rays in Figure 6.18, the cracks are slightly longer in the filled hole specimen. There was also more off-axis cracking and surface wear around the hole. Cracking at the top and bottom of the notch in the filled hole specimen occurred at the highest stress reached. It was likely due to stress transfer across the hole and Poisson effects causing localized compression in the transverse direction.

A) 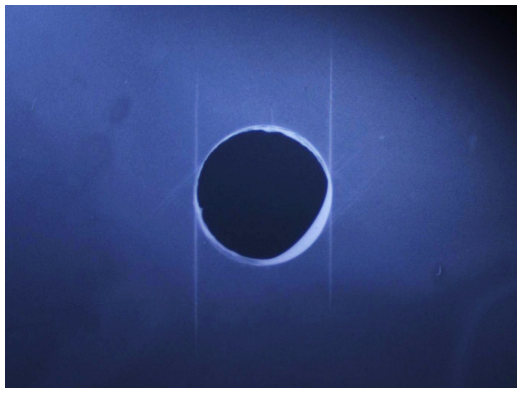 B) 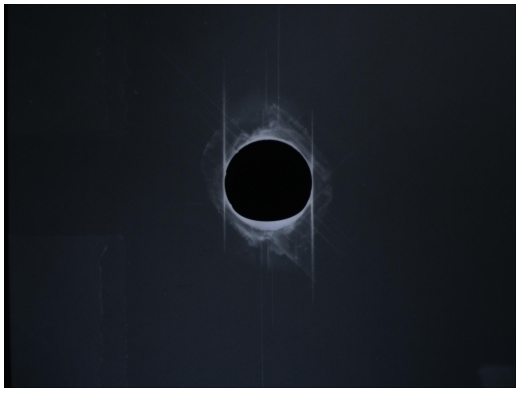

Figure 6.18 Radiographic images around 6.35mm diameter notch after 1 million cycles at max stress Mostly Compression for a) Open Hole specimen, b) Filled Hole specimen

6.5.2 80/20 Laminate (R = -3)

Comparing the 80/20 laminate in Open versus Filled Hole Mostly Compression Stress, the filled hole test withstood an extra increment of stress (compared to the open hole test) before seeing damage initiation. As in other tests, the filled hole test showed a slower crack growth rate throughout the test procedure. While the filled hole test had a slightly greater crack growth during the long-term fatigue test portion of the Damage Initiation Method, it happened at a much higher stress than the open hole test. See Figure 6.19. The data is normalized to the static ultimate compressive strength of the 80/20 composite laminate.

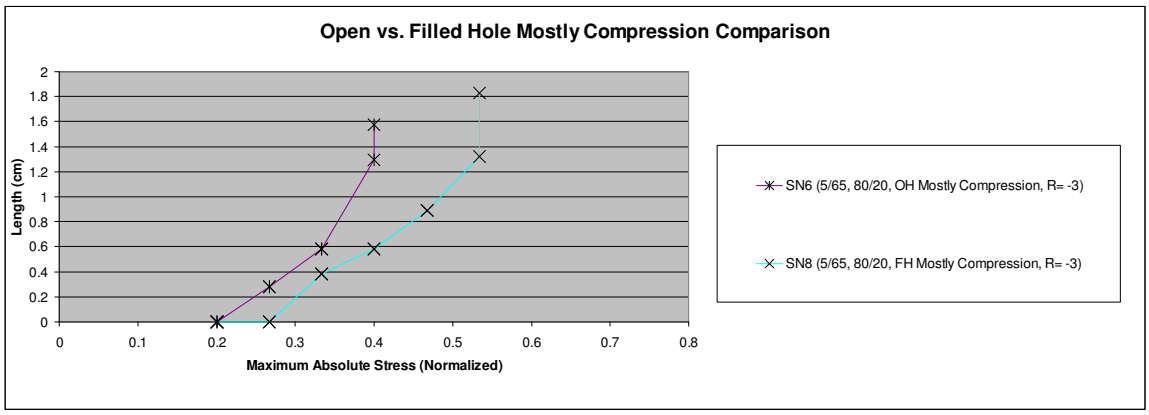

Figure 6.19 Open versus Filled Hole Mostly Compression tests (Specimen, Layup, Test type, R ratio)

As seen in the x-rays in Figure 6.20, the cracks are slightly longer in the filled hole specimen. The only off-axis cracking visible was a 65° crack extending all the way to the edge of the specimen. This was the only test in which this type of damage occurred.

Cracking occurred at the top and bottom of the notch in the filled hole specimen. It was likely due to stress transfer across the hole and Poisson effects causing localized compression in the transverse direction.

A) 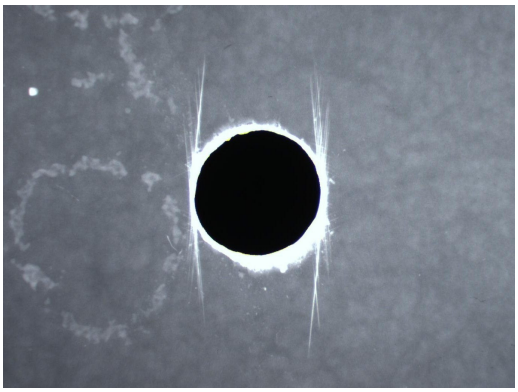 B) 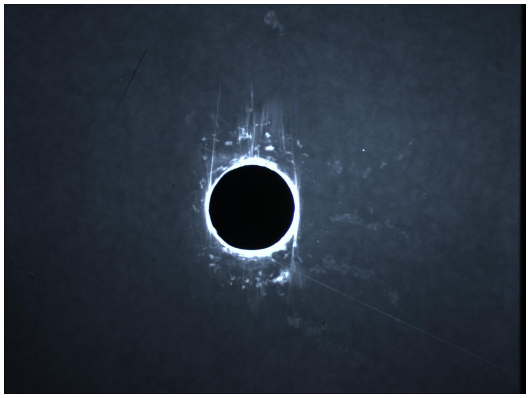

Figure 6.20 Radiographic images around 6.35mm diameter notch after 1 million cycles at max stress Mostly Compression for a) Open Hole specimen, b) Filled Hole specimen

Chapter 7 : STRESS RATIO COMPARISONS

This section will discuss the split length differences across the various stress ratios at which each laminate was tested.

7.1 50/40/10 Laminate – Open Hole Testing

Comparisons within laminates show the effect of R ratios on the composite's performance. In direct contrast to metals, composites generally perform better in tension than in compression due to issues specific to that material system – namely microbuckling and kink banding [27]. Consequently, Open Hole Tension specimens withstood higher stresses before showing the same damage state as Open Hole Compression laminates at lower fatigue stresses. The open hole tension specimen withstood a 33% higher absolute maximum stress than the open hole compression test. The Mostly Tension specimen performed 25% better than the Mostly Compression specimen. In terms of maximum stress achieved, the ranking from best to worst was as follows: Open Hole Tension, Mostly Tension, Open Hole Compression, Mostly Compression, Fully Reversed. Figure 7.1 shows the five different tests run for the 50/40/10 laminate.

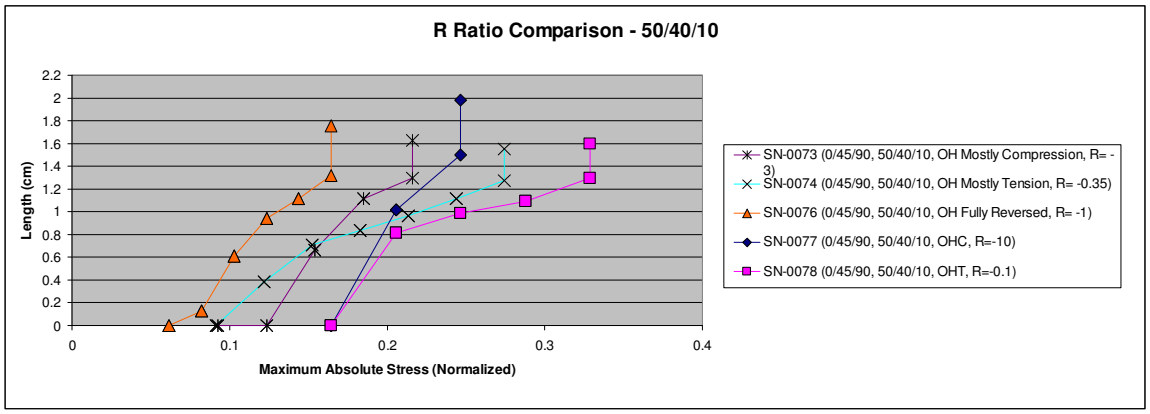

Figure 7.1 50/40/10 Open Hole Laminate tests (Specimen, Layup, Test type, R ratio)

Regardless of the stress ratio each specimen was tested at, they all reached the same characteristic damage state. While the tests with significant tension displayed more linear damage accumulation, all tests showed dominant longitudinal splitting augmented with minor cracking in the 45° plies. This can be seen in Figure 7.2.

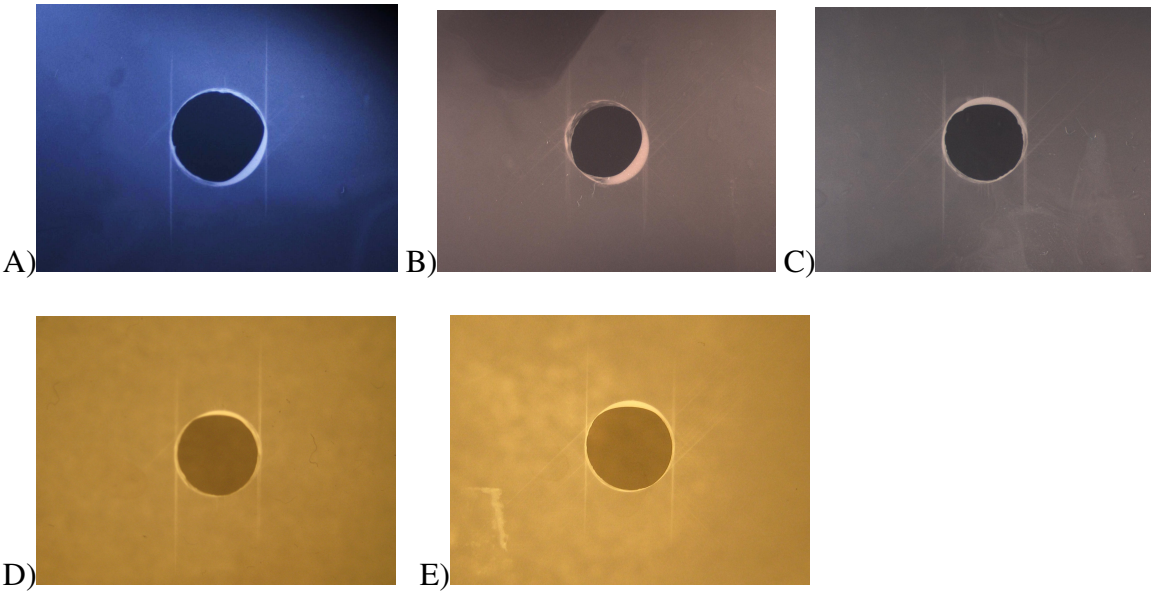

Figure 7.2 Open Hole testing after 1 million cycles at max stress for a) Mostly Compression, b) Mostly Tension, c) Fully Reversed, d) Compression, e) Tension

7.2 50/40/10 Laminate – Filled Hole Testing

Filled Hole testing for 50/40/10 laminates at different stress ratios highlighted the differences between each specimen's damage resistance to incremental stress levels as well as long-term crack growth suppression. For this round of tests run according to the Damage Initiation Concept, the filled hole tests showed a more linear damage progression than open hole specimens as well as achieving a higher maximum stress. When considering maximum stress reached, the laminates rank (best to worst): Filled Hole Tension, Filled Hole Mostly Tension, Filled Hole Mostly Compression, Filled Hole Compression, Filled Hole Fully Reversed. In Figure 7.3, the data from each laminate tracks the specimens' tests.

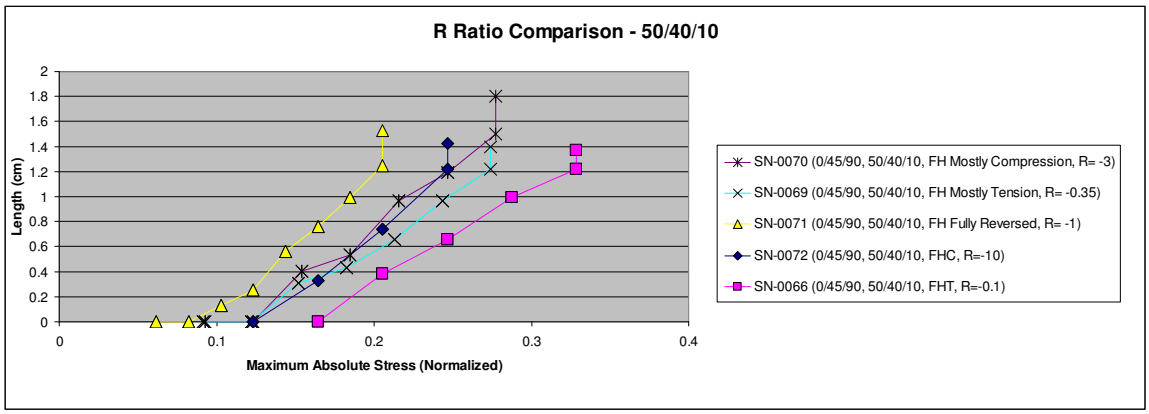

Figure 7.3 50/40/10 Filled Hole Laminate tests (Specimen, Layup, Test type, R ratio)

The damaged areas around the central hole in the coupon specimen were similar, with only slight differences. One interesting note was that increased amounts of tension corresponded to increased cracking in the off-axis 45° plies. The Tension test had the most, followed by the Mostly Tension test, the Fully Reversed one, and the two compression tests. See Figure 7.4 for the x-rays.

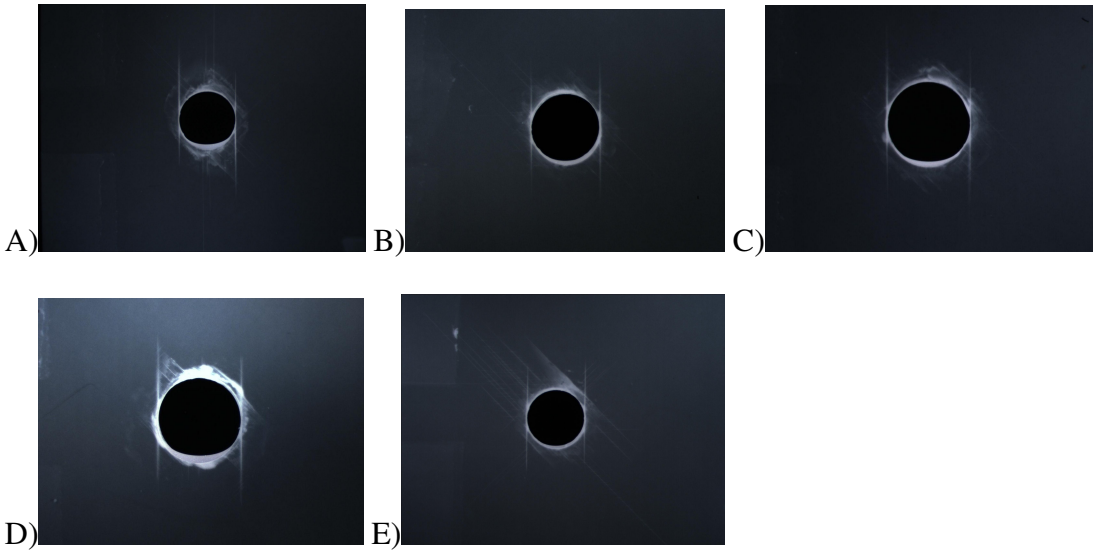

Figure 7.4 Filled Hole testing after 1 million cycles at max stress for a) Mostly Compression, b) Mostly Tension, c) Fully Reversed, d) Compression, e) Tension

7.3 80/20 Non-Traditional Laminate – Open Hole Testing

The 80/20 non-traditional laminate with 80% longitudinal plies (±5°), also exhibited the same trends when comparing across different R ratios as shown in Figure 7.5. In this case, there was a 16% increase in maximum absolute stress for the Tension specimen as compared to the Compression one. While the Tension specimen initiated damage first, it reached a higher stress. The long-term fatigue damage growth rate was almost identical. There was a 48% increase in absolute maximum stress for the Mostly Tension specimen when compared to the Mostly Compression one.

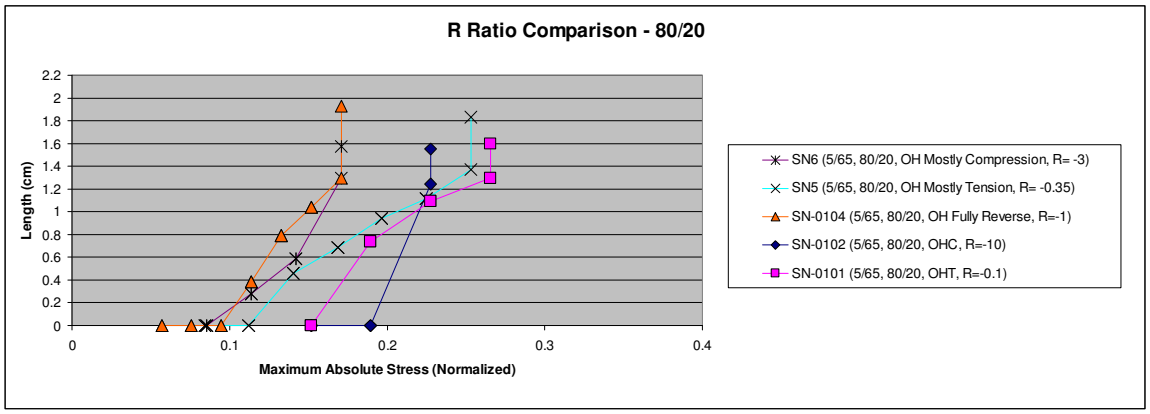

Figure 7.5 80/20 Open Hole Laminate tests (Specimen, Layup, Test type, R ratio)

Looking at the x-rays of the open hole tests in Figure 7.6, one can see that all the tests have longitudinal splitting, with no off-axis cracks. The only difference was minor changes in length of the final split.

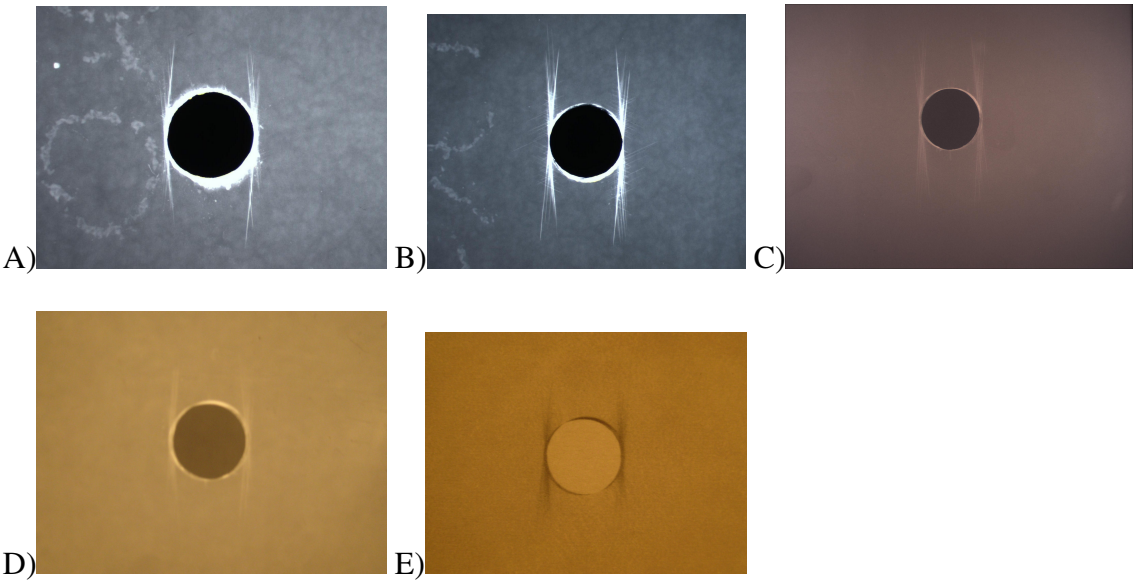

Figure 7.6 Open Hole testing after 1 million cycles at max stress for a) Mostly Compression, b) Mostly Tension, c) Fully Reversed, d) Compression, e) Tension

7.4 80/20 Non-Traditional Laminate – Filled Hole Testing

The Filled Hole tests run for the 80/20 non-traditional laminates are recorded in Figure 7.7. In terms of maximum stress reached, the laminates rank (best to worst): Filled Hole Compression, Filled Hole Mostly Tension, Filled Hole Tension, Filled Hole Mostly Compression, Filled Hole Fully Reversed. The Compression test experienced a 16% higher load than the Tension test. The Mostly Tension test withstood a 10% greater load than the Mostly Compression test.

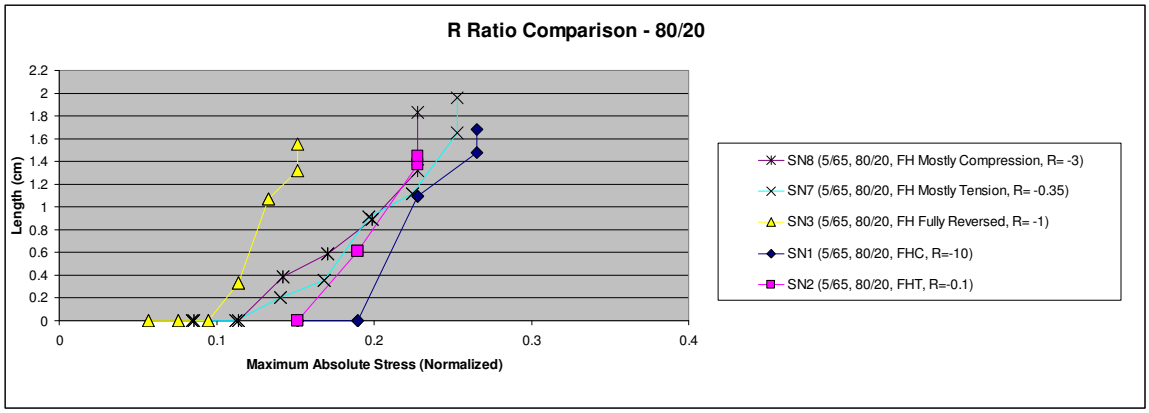

Figure 7.7 80/20 Filled Hole Laminate tests (Specimen, Layup, Test type, R ratio)

When examining the final damage states of the specimens using radiography, a couple interesting facts emerged. First, all the specimens split to the left and right of the hole, as expected. Second, all the tests, except for the Filled Hole Compression test, displayed splitting originating from the top and bottom of the hole. This is like due to a combination of stress transfer across the hole and localized compression due to Poisson effects. The radiographic images are shown in Figure 7.8.

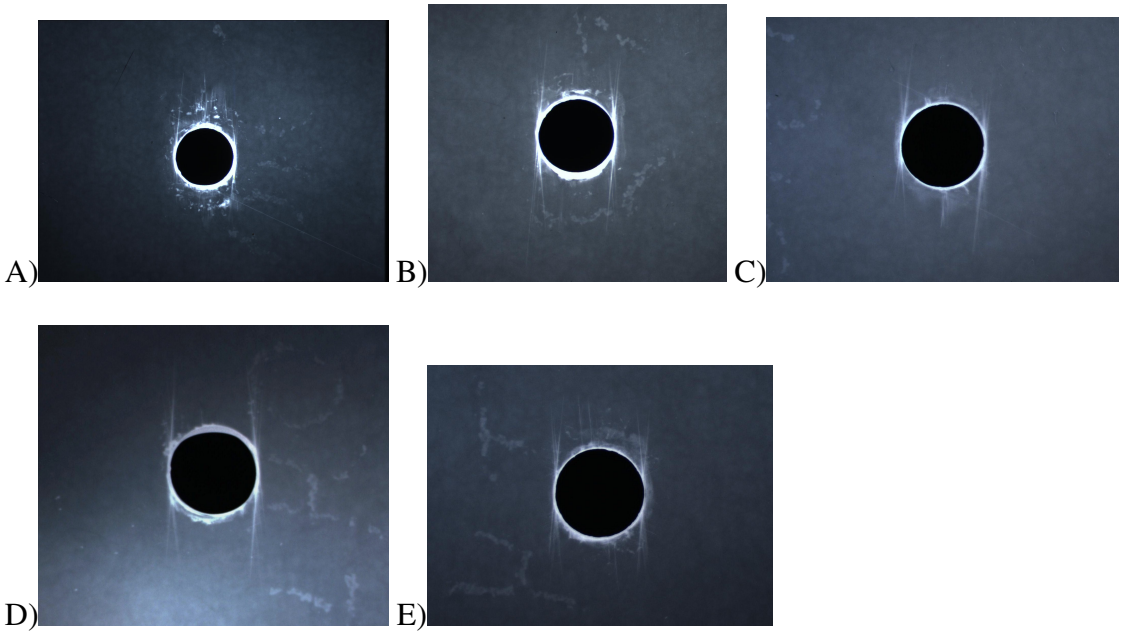

Figure 7.8 Filled Hole testing after 1 million cycles at max stress for a) Mostly Compression, b) Mostly Tension, c) Fully Reversed, d) Compression, e) Tension

7.5 70/30 Non-Traditional Laminate – Open Hole Testing

Comparing the tests for the 70/30 non-traditional laminate with 70% longitudinal plies (±5°), a 17% increase in maximum stress was recorded for the Open Hole Tension test compared to the Open Hole Compression test as displayed in Figure 7.9. While the tensile specimen initiates damage at a lower stress level, its growth is slower than the compressive test, and consequently reaches a higher stress level before split reaches the critical length of 1.27 cm (0.50”).

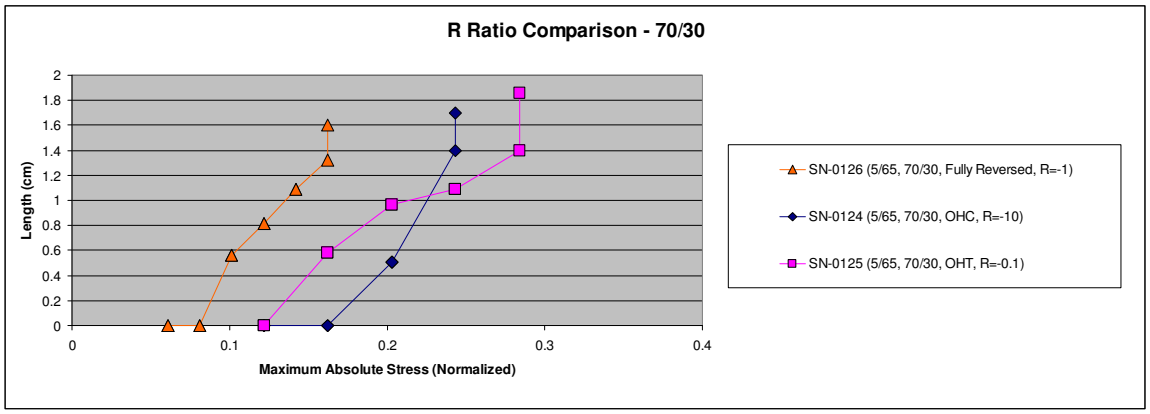

Figure 7.9 70/30 Open Hole Laminate tests (Specimen, Layup, Test type, R ratio)

In Figure 7.10, all three tests showed the same characteristic damage state after completion of the Damage Initiation test – which includes incremental stress as well as long-term crack growth. The only difference was the stress level after which the x-ray was taken.

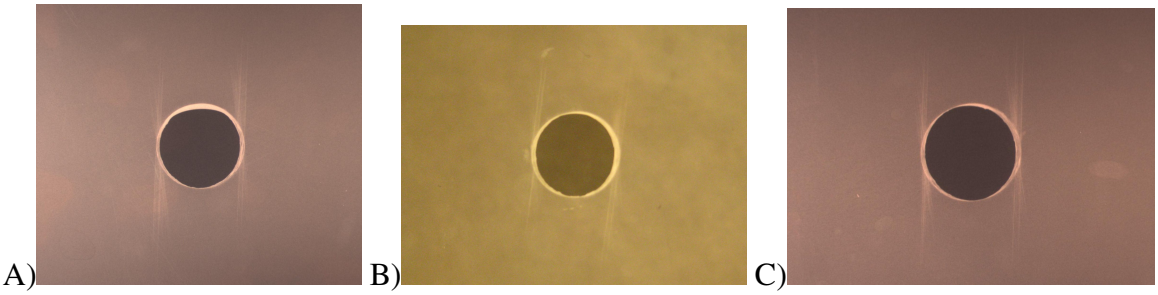

Figure 7.10 Open Hole testing after 1 million cycles at max stress for a) Fully Reversed, b) Compression, c) Tension

7.6 Other Ways to Plot Data

All the graphs presented showed the data plotted against the absolute value of the maximum stress the specimen experienced. For the comparisons within stress ratios or

between filled and open holes, this makes no difference. The problem is encountered when comparing across the five stress ratios used in this test matrix. Various other graphs were created to plot against the true maximum stress, the stress range, and the square root of the absolute max stress times the stress range. The absolute value of the stress was chosen for a couple reasons. The true maximum stress graph was misleading, in that the tests with significant compressive stress appeared to be under low stress since only the small tension portion was plotted. The stress range graph was discarded, because across laminates there were no clear trends. The "square root of the absolute max stress times the stress range" was likewise inconclusive, due to its reliance on the stress range. The graphs shown below are for the 50/40/10 laminate.

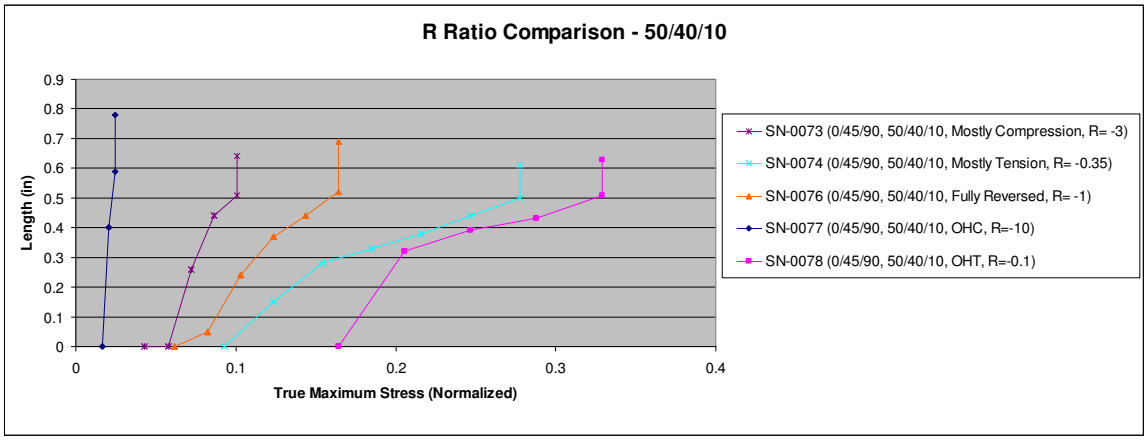

Figure 7.11 True Maximum Stress Graph of 50/40/10 Open Hole Laminate tests (Specimen, Layup, Test type, R ratio)

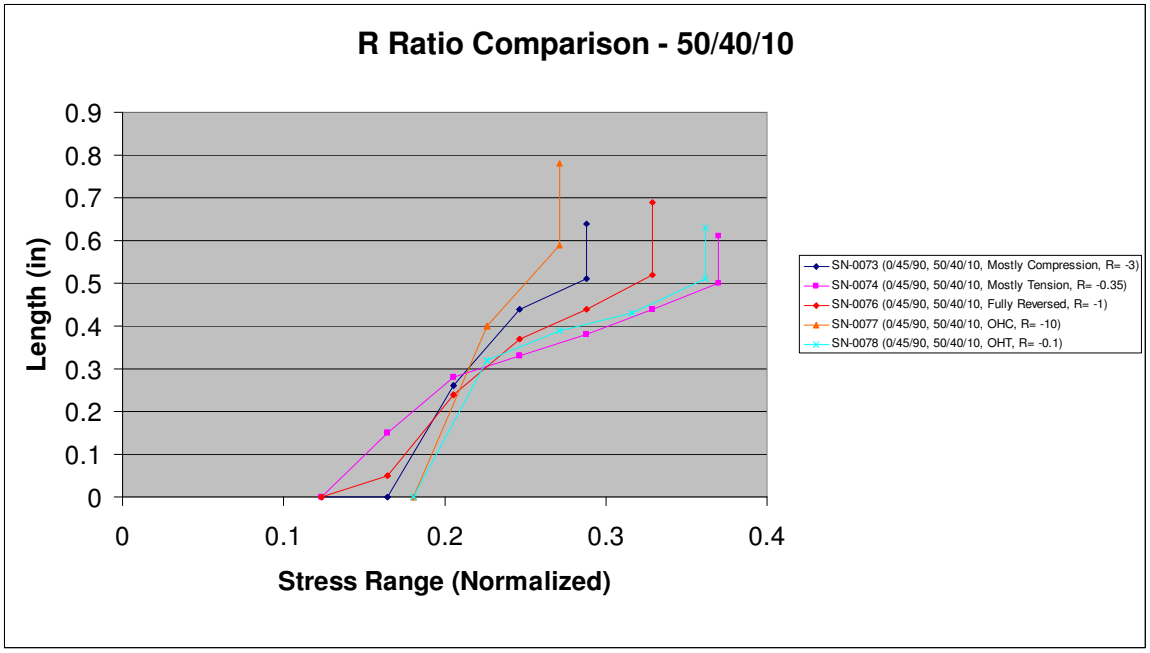

Figure 7.12 Stress Range Graph of 50/40/10 Open Hole Laminate tests (Specimen, Layup, Test type, R ratio)

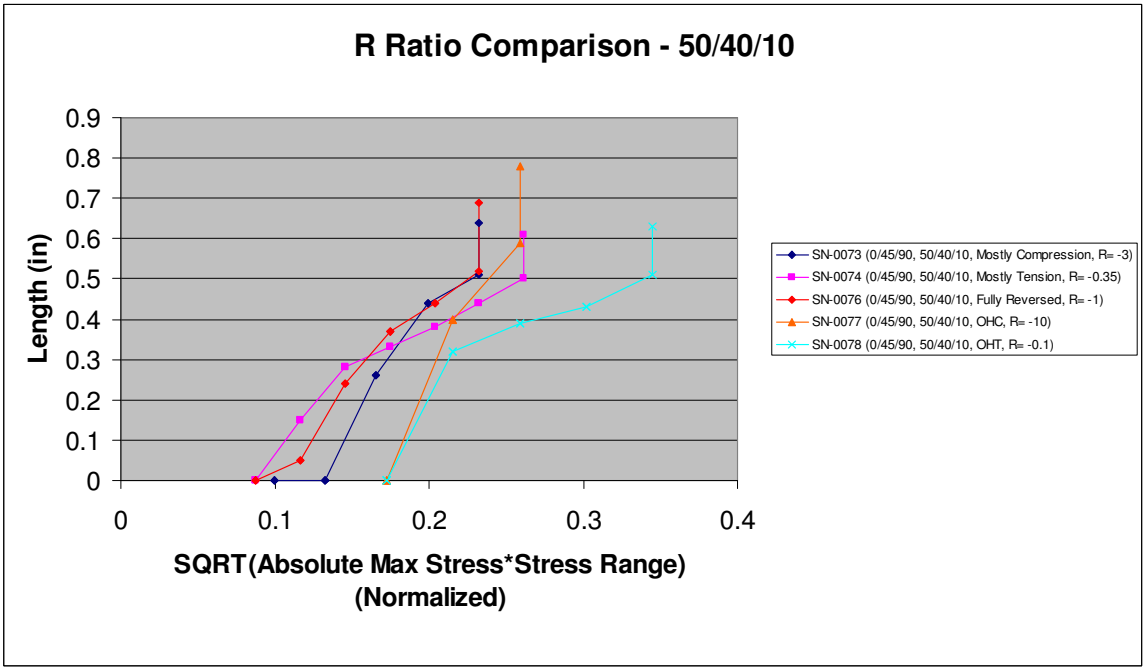

Figure 7.13 Square Root Graph of 50/40/10 Open Hole Laminate tests (Specimen, Layup, Test type, R ratio)

Chapter 8 : SUMMARY AND CONCLUSIONS

This section contains the summary of test variables as well as conclusions drawn from the testing.

8.1 Summary of Test Variables

The following section discusses the effects of the variables in this test matrix – specifically the type of layup, R values (stress ratios), and stress levels.

8.1.1 Type of Layup

The effects of the layup were significant, even at relatively short split lengths. Between the two non-traditional layups, the one with 80% longitudinal plies (80/20) had shorter split lengths at the same stress level than the 70/30 layup for all the stress ratios run. The 70/30 specimen withstood a higher percentage of its ultimate stress before the damage criterion of 1.27cm (0.50") signaled the start of the long-term crack growth portion of the test.

Comparing the traditional layup with the non-traditional, the traditional outperformed the other two in Tension, but was the worst in Compression. The slightly off-axis plies are not as stiff as 0° plies, and could be susceptible to a scissor-like action that slightly tries to align them under tension. Under compression, there is no mechanism that would match this behavior. Even at small splits, the off-axis plies appear to stabilize the crack growth. At longer splits and under higher stresses, this effect would be amplified.

8.1.2 Stress ratios and stress levels

The stress ratios, R values, played a significant role in determining the highest stress level a composite specimen could handle without reaching the damage criterion that represented critical damage. Since composites have less damage modes affecting them in tension than in compression, stress ratios with greater percentages of tension during the fatigue cycle performed better. At the same stress level, the compression test laminates displayed a longer crack length. At longer crack lengths, the tension laminates could withstand a higher stress level.

8.1.3 Open versus Filled Holes

For the open versus filled hole comparisons, a couple important distinctions were made. First, there was cracking at the top and bottom of the hole for the filled hole tests that was not present in the open hole tests. This was due to stress transfer across the hole through the fastener and Poisson effects. Second, the filled hole tests performed as good or better for most of the stress ratios. While the open hole tests looked slightly better on a couple stress ratios, this could be due to statistical error.

8.2: Conclusions

Two non-traditional carbon fiber composite laminates ($[\pm5/65/(\pm5)_2/-65/\pm5]_s$ and $[\pm5/65/(\pm5)_2/-65/5/65]_s$) were compared with a more traditional composite laminate ($[45/90/-45/0_2/45/0_2/-45/0]_s$) Their damage states were assessed through the use of in-situ radiography at predetermined intervals. Varying the stress ratio and stress level lent insight into finding the stress level for damage initiation and stress required for a 1.27cm

long damaged area. The calculated stress concentrations, from the Lekhnitskii equation, were not able to predict which laminate would withstand the highest loading.

For Cyclic Open Hole Tension (R=-0.1), the traditional laminate slightly outperformed the traditional laminates by reaching a higher stress level before accumulating a critical damage. This was the same trend for the Filled Hole Tension tests. For Cyclic Open Hole Compression (R=-10), the non-traditional laminates were the best at suppressing damage under fatigue loading. In the Filled Hole Compression test, the traditional 50/40/10 did better. With Fully Reversed testing (R=-1), the 80/20 performed better with open holes while the 50/40/10 performed better with filled holes. In Mostly Tension (R=-0.35), the 50/40/10 and 80/20 were similar in open hole testing, but the 50/40/10 did better with filled holes. For Mostly Compression (R=-3), the 50/40/10 was better with open or filled holes. Within each laminate, comparing predominantly tension cycling with mostly compression cycling, the tension tests allowed the composite to reach a higher maximum absolute stress level. However, damage usually initiated in the tension specimen first, but had a slower growth rate.

Chapter 9 : RECOMMENDATIONS FOR FUTURE WORK

Non-traditional laminates show promise for specific applications, specifically those that are compression dominated. Composite design requires a careful balance of different properties. A slight loss in stiffness due to off-axis plies might be offset by a higher damage resistance that arrests cracks beyond a certain length.

The end result of this research is to understand the damage progression in non-traditional laminates during fatigue loading and acquire data useful for developing models to accurately predict the damaged zone at a given cycle count, specifically for the 5°(80%)/65°(20%), 5°(70%)/65°(30%), 0°(50%)/45°(40%)/90°(10%), and 0°(80%)/45°(10%)/90°(10%) layups. Due to +5°/-5° plies overlapping, it is hoped that the non-traditional laminates (in which the primary load-carrying fibers are not 0° fibers, but slightly off the longitudinal axis) will stunt the damage progression by not providing a clear path for cracks or splits to propagate. In design cases desiring notched composites in uniaxial tension or compression, the non-traditional laminates could have the most impact due to superior damage suppression around the notch.

APPENDIX A

This appendix contains the test matrix used for this project, and shows the available comparisons between layups and test conditions.

Table 0.1: Test Matrix

Fatigue Initiation

	5/65 (80/20)		50/40/10		5/65 (70/30)
	OH	FH-HC	OH	FH-HC	OH
R = -0.1	x	x	x	x	x
R = -10	x	x	x	x	x
R = -0.35	x	x	x	x	
R= -3.0	x	x	x	x	
R= -1.0	x	x	x	x	x

Total Test: 23

REFERENCES

[1] Treasurer, P.J. and Johnson, W.S., *Radiographic Investigation of the Effects of Ply Modification on Damage Development in Laminates Containing Circular Holes,* approved for Journal of Composite Materials.

[2] Berbinau, P., *Effect of off-axis ply orientation on 0°-fibre microbuckling*. Composites – Part A: Applied Science and Manufacturing, 1999. 30: p. 1197-1207.

[3] Yan, Y., et al., *Experimental study on clamping effects on the tensile strength of composite plates with a bolt-filled hole.* Composites - Part A: Applied Science and Manufacturing, 1999. **30**(10): p. 1215-1229.

[4] Spearing, S.M., *Fatigue damage mechanics of composite materials. I: Experimental measurement of damage and post-fatigue properties.* Composites Science and Technology. 44: p. 159-168.

[5] Talreja, Ramesh, *Damage Mechanics and Fatigue Life Assessment of Composite Materials*. International Journal of Damage Mechanics, 1999. Volume 8, p. 339-354

[6] Kellas, S., *Fatigue Damage Development in a Notched Carbon Fibre Composite*. Composite Structures, 1986, Volume 5, p. 143-157.

[7] Barboni, R., *The Effects of Delamination on the Fatigue Behavior of Composite Structures*. Journal of Composite Materials, 1999, Volume 33, No. 3, p. 267-303.

[8] Razvan, A.; Bakis, C.E.; and Reifsnider, K.L.; *Influence of Load Levels on Damage Growth Mechanisms of Notched Composite Materials*. Composite Materials, Volume 9, p. 371-389.

[9] Niu, K. and Talreja, R., *Modeling of compressive failure in fiber reinforced composites*. International Journal of Solids and Structures, 2000. 37: p. 2405-2428.

[10] ASTM Standards., *Standard Test Method for Open-Hole Compressive Strength of Polymer Matrix Composite Laminates.* Designation D6484/D6484M-04. Section 15: p. 356-370.

[11] Boeing_Document_No._D6-83079-71, *Test Method for Compressive Properties of Thin Composite Lamina and Laminates*. 2003, Boeing: Seattle, WA.

[12] Turcic, Branko, *Fatigue Damage Periods in Composite Laminates*. Materials Science and Engineering. A130: p. 17-20.

[13] Maier, G., *Notch sensitivity of multidirectional carbon fibre-reinforced polyimides in fatigue loading as a function of stress ratio*. Composites, 1987. Volume 18, No. 5.

[14] Li, L.X., Wang, T.J., *A Unified Approach to Predict Overall Properties of Composite Materials*. Materials Characterization, 2005. **54**: p. 49-62.

[15] Xi, Y., Eskandari-Ghadi, M., *Damage Theory Based on Composite Mechanics*. Journal of Engineering Mechanics, 2006. November: p. 1195-1204

[16] Hashin, Z., *Failure Criteria for Unidirectional Composites.* Journal of Applied Mechanics, 1980. **47**: p. 329-334.

[17] Billups, E.K., Cavalli, M.N., *2D Damping Predictions of Fiber Composite Plates: Layup Effects*. Composites Science and Technology, 2008. **68**: p. 727-733.

[18] Wall, P., *A Comparison of Homogenization, Hashin-Shtrikman Bounds and the Halpin-Tsai Equations*. Applications of Mathematics, 1997. **42**: No.4, p. 245-257.

[19] Tan, H., Huang, Y., *Constitutive Behaviors of Composites with Interface Debonding: the Extended Mori-Tanaka Method for Uniaxial Tension*. Spring Science + Business Media, 2007. November: p. 139-148.

[20] Hart-Smith, L.J., *Predictions of a Generalized Maximum Shear Stress Failure Criterion for Certain Fibrous Composite Laminates*. Composites Science and Technology, 1998. **58**: p. 1179-1208.

[21] Tsai, S.W. and E. Wu, *A General Theory of Strength for Anisotropic Materials.* Journal of Composite Materials, 1971. **5**: p. 55-80.

[22] Waddoups, M.E., J.R. Eisenmann, and B.E. Kaminski, *Macroscopic Fracture Mechanics of Advanced Composite Materials.* Journal of Composite Materials, 1971. **5**: p. 446-454.

[23] Whitney, J.M. and R.J. Nuismer, *Stress Fracture Criteria For Laminated Composites Containing Ss Concentrations.* Journal of Composite Materials, 1974. **8**: p. 253-265.

[24] Karlak, R.F., *Hole Effects in a Related Series of Symmetrical Lamiantes*, in *Procedings of Failure Modes of Composites, IV*. 1977, The Metallurgical Society of AIME: Chicago. p. 105-117.

[25] Konish, Jr. H.J., Swedlow, J.L., Cruse, T.A., *Fracture Phenomena in Advanced Fiber Composite Materials*. AIAA Journal, 1974, Volume 11, No. 1, p. 40-43.

[26] Rice, J.R., *A Path Independent Integral and the Approximate Analysis of Strain Concentrations by Notches and Crack.* Journal of Applied Mechanics, 1968, Vol. 35, No. 2., p. 379-386.

[27] Spearing, S.M., *Fatigue damage mechanics of composite materials. II: A Damage growth model.* Composites Science and Technology. 44: p. 169-177.

[28] Shokrieh, Mahmood M., *Progressive Fatigue Damage Modeling of Composite Materials, Part I: Modeling*. Journal of Composite Materials. Volume 34, No. 13/2000.

[29] Shokrieh, Mahmood M., *Progressive Fatigue Damage Modeling of Composite Materials, Part II: Material Characterization and Model Verification*. Journal of Composite Materials. Volume 34, No. 13/2000.

[30] Adam, T., *A Power Law Fatigue Damage Model for Fiber-Reinforced Plastic Laminates*. Proceedings of the Institution of Mechanical Engineers, Part C: Mechanical Engineering Science, 1986, Volume 200, No. C3, p. 155-156.

[31] Turcic, Branko, *"Natural" Phenomenological Fatigue Damage Cumulation Model for Composite Laminates*. Materials Science and Engineering. A130: p. 17-20.

[32] Reifsnider, K.L., *The Critical Element Model: A Modeling Philosophy*. Engineering Fracture Mechanics, Volume 25, No. 5/6, p. 739-749.

[33] Etheridge, A., *Investigation of Progressive Damage and Failure in IM7 Carbon Fiber/5250-4 Bismaleimide Resin Matrix Composite Laminates.* Georgia Tech MS Thesis, 1998.